UNCLASSIFIED

AD NUMBER
AD507040
CLASSIFICATION CHANGES
TO: **UNCLASSIFIED**
FROM: **CONFIDENTIAL**
LIMITATION CHANGES
TO: **Approved for public release; distribution is unlimited.**
FROM: **Distribution authorized to U.S. Gov't. agencies and their contractors; Critical Technology; NOV 1969. Other requests shall be referred to Air Force Rocket Propulsion Laboratory, Attn: RPPR-STINFO, Edwards AFB, CA 93523. This document contains export-controlled technical data.**
AUTHORITY
10 dec 1985, AFRPL Ltr 13 jan 86, AFRPL ltr

THIS PAGE IS UNCLASSIFIED

REPRODUCED AT GOVERNMENT EXPENSE

AD 507 040

AUTHORITY:
AERL Ltr 10 Dec 85

GENERAL DECLASSIFICATION SCHEDULE

IN ACCORDANCE WITH
DOD 5200.1-R & EXECUTIVE ORDER 11652

THIS DOCUMENT IS:

CLASSIFIED BY_____

Subject to General Declassification Schedule of Executive Order 11652-Automatically Downgraded at 2 Years Intervals-DECLASSIFIED ON DECEMBER 31,

BY

Defense Documentation Center
Defense Supply Agency
Cameron Station
Alexandria Virginia 22314

THIS REPORT HAS BEEN DELIMITED
AND CLEARED FOR PUBLIC RELEASE
UNDER DOD DIRECTIVE 5200.20 AND
NO RESTRICTIONS ARE IMPOSED UPON
ITS USE AND DISCLOSURE.

DISTRIBUTION STATEMENT A

APPROVED FOR PUBLIC RELEASE;
DISTRIBUTION UNLIMITED.

SECURITY MARKING

The classified or limited status of this report applies to each page, unless otherwise marked.
Separate page printouts MUST be marked accordingly.

THIS DOCUMENT CONTAINS INFORMATION AFFECTING THE NATIONAL DEFENSE OF THE UNITED STATES WITHIN THE MEANING OF THE ESPIONAGE LAWS, TITLE 18, U.S.C., SECTIONS 793 AND 794. THE TRANSMISSION OR THE REVELATION OF ITS CONTENTS IN ANY MANNER TO AN UNAUTHORIZED PERSON IS PROHIBITED BY LAW.

NOTICE: When government or other drawings, specifications or other data are used for any purpose other than in connection with a definitely related government procurement operation, the U.S. Government thereby incurs no responsibility, nor any obligation whatsoever; and the fact that the Government may have formulated, furnished, or in any way supplied the said drawings, specifications, or other data is not to be regarded by implication or otherwise as in any manner licensing the holder or any other person or corporation, or conveying any rights or permission to manufacture, use or sell any patented invention that may in any way be related thereto.

CONFIDENTIAL

AFRPL-TR-69-246

ORIGINAL CONTAINS COLOR PLATES: ALL DDC REPRODUCTIONS WILL BE BLACK AND WHITE. ORIGINAL MAY BE SEEN IN DDC HEADQUARTERS

AD507040

CRYSTAL LATTICE DOPING STUDIES OF HIGH ENERGY PROPELLANT INGREDIENTS (U)

Final Report

Drs. J. Norman Maycock, V. R. Pai Verneker and M. McCarty, Jr.

Research Institute for Advanced Studies
Martin Marietta Corporation
1450 South Rolling Road
Baltimore, Maryland 21227

September 1969

DDC
RECEIVED
FEB 16 1970

Group IV
Downgraded at 3-Year Intervals
Declassified After 12 Years
DOD DIR. 5200. 10

In addition to security requirements which must be met, this document is subject to special export controls and each transmittal to foreign governments or foreign nationals may be made only with prior approval of AFRPL (RPPR-STINFO), Edwards, California 93523.

This material contains information affecting the national defense of the United States within the meaning of the espionage laws, Title 18, U. S. C., Sections 793 and 794, the transmission or revelation of which in any manner to an unauthorized person is prohibited by law.

Air Force Rocket Propulsion Laboratory
Directorate of Laboratories
Edwards, California
Air Force Systems Command, United States Air Force

CONFIDENTIAL

AFRPL-TR-69-246 **CONFIDENTIAL** COPY NO.

i

Crystal Lattice Doping Studies of High Energy Propellant Ingredients (U)

Final Report

Prepared by

Drs. J. Norman Maycock, V. R. Pai Verneker and M. McCarty, Jr.

RIAS TR-69-12c

Research Institute for Advanced Studies
(RIAS)
Martin Marietta Corporation
1450 South Rolling Road
Baltimore, Maryland 21227

September 1969

Sponsoring Organization
U.S.A.F. Rocket Propulsion Laboratory, Edwards A.F.B.
Edwards, California

Contract No. F04611-68-C-0068

In addition to security requirements which must be met, this document is subject to special export controls and each transmittal to foreign governments or foreign nationals may be made only with prior approval of AFRPL (RPPR/STINFO), Edwards, California 93523.

NOTICES

(U) When Government drawings, specifications, or other data are used for any purpose other than in connection with definitely related Government procurement operation, the United States Government thereby incurs no responsibility nor any obligation whatsoever; and the fact that the Government may have formulated, furnished, or in any way supplied the said drawings, specifications or other data, is not to be regarded by implication or otherwise as in any manner licensing the holder or any other person or corporation, or conveying any rights or permission to manufacture, use, or sell any patented invention that may in any way be related thereto.

This document is subject to special export controls and each transmittal to foreign governments or foreign nations may be made only with prior approval of Air Force Rocket Propulsion Laboratory, Edwards, California 93523.

FOREWORD

(U) This technical report was prepared for the U. S. Air Force Rocket Propulsion Laboratory, Edwards A.F.B., by the Research Institute for Advanced Studies (RIAS), Martin Marietta Corporation, Baltimore, under contract No. F04611-68-C-0068. This Final Report covers the period May 1, 1968 through August 31, 1969. At various times the Air Force monitors were Capts. R. Bargmeyer, W. Anders and Lt. F. Clark.

(U) The authors gratefully acknowledge the assistance of C. S. Gorzynski, Jr., L. L. Rouch and H. W. Lochte (RIAS) during the tenure of this program.

(U) The Contractor's report number is RIAS TR-69-12c.

(U) This report has been distributed according to the CPIA distribution list dated May 1967, as amended.

(U) This report was submitted for approval September 1969.

(U) This technical report has been reviewed and is approved by:

W. H. EBEIKE, Colonel, USAF
Chief, Propellant Division

ABSTRACT

(C) The kinetics of the thermal decomposition of both pure and Mg doped AlH_3 have been determined, by using both isothermal constant volume and simultaneous DTA-TGA techniques. Of most importance in these derived parameters is the fact that the activation energy for these thermal decomposition of the Mg doped AlH_3 is different from that for the pure AlH_3. To help resolve these discrepancies the electrical conductance of these same samples has also been measured as a function of temperature and time. From these two studies a model for the thermal decomposition of AlH_3 has been developed. Also reasons for the effectiveness of Mg in increasing the thermal stability of AlH_3 are presented.

(U) The thermal behavior of both Thiokol and Navy manufactured HAP has been investigated by simultaneous DTA-TGA, thermal microscopy and mass spectrometry between room temperature and 100°C. These techniques clearly establish that HAP undergoes a crystal phase change at 65°C which is slowly reversible on cooling. At this same temperature H_2O is evolved, presumably due to the crystal relaxation during the phase change. A unique feature of these samples is that they contain spherical "pockets" of some material having a higher refractive index than the host molten HAP. At the moment the identity of this material is uncertain although it could be a saturated aqueous solution of HAP, perchloric acid or hydroxylamine. The poor compatibility of HAP above the crystal phase change is attributed to volatile species being liberated at the phase change. These volatiles could then disturb the HAP-binder interface bonding.

TABLE OF CONTENTS

LIST OF TABLES

LIST OF FIGURES

LIST OF FIGURES (contd)

UNCLASSIFIED

PART 1

Thermal Stability of Aluminum Hydride (U)

UNCLASSIFIED

1.1. Background and Objective (U)

(U) Five forms of aluminum hydride have been reported in the literature. A short lived species, AlH, has been produced by an electrical discharge technique and has been used to provide a measurement of the Al-H bond length (1.648Å).[1] A polymerized hydride $(AlH_3)_n$ has been claimed by Stecher and Wiberg[2] but has also been disputed by Finholt et al.[3] This preparation is based on $LiAlH_4$ and $AlCl_3$ in an ether solution. Appel and Frankel[4] have also produced a non solvated AlH_3 by bombarding an ultrapure aluminum target with hydrogen ions. Gaseous AlH_3 and its dimer have been produced in both a static and flowing system where aluminum from a hot tungsten filament is evaporated into hydrogen at low pressures and the product is trapped out at -195°C.[5,6] Finally, recent work at the Dow Chemical Co.[7] has resulted in the production of five crystalline forms of non solvated aluminum hydride. Of these five forms, one designated "1433" appears to be similar to a preparation by Rice and Chizinsky.[8] A second form, designated "1451" appears to be similar to the preparation of Appel and Frankel.[4] Of these five forms the type "1451" is the most thermally stable. An X-ray study of "1451" by Turley and Rinn[7] shows that it crystallizes with a trigonal space group $R\bar{3}c$ with six molecules in an hexagonal unit cell of dimensions $\underline{a}$ = 4.449Å; $\underline{c}$ = 11.804Å. They have also shown that each Al participates in six three-center Al-H-Al bonds to six surrounding H spirals forming hydrogen bridges to three Al in the plane above and three in the plane below.

(U) A somewhat impure AlH_3 (95% weight impurity) has been used by Sinke et al[9] for the determination of its fundamental thermodynamic parameters. From the heat of formation and the absolute entropy they calculated the Gibbs energy of formation to be $\Delta G_{298^oK} = 11.11 \pm 0.23$ kcal $mole^{-1}$ which predicts that AlH_3 should be highly unstable with respect to decomposition into its elements.

(U) Presently there has been no report of the thermal decomposition kinetics and mechanisms of AlH_3 in the literature. With the previously discussed properties of AlH_3 in mind we are reporting on a study of its thermal decomposition. This decomposition study has been carried out on the "1451" phase of AlH_3 by both isothermal and simultaneous differential thermal and thermogravimetric (DTA-TGA) analysis technique. A model for the decomposition consistent with the experimental data is also presented.

1.2. Experimental Procedures (U)

1.2.1. Materials.

(C) Pure AlH_3 (phase 1451) was supplied by the Dow Chemical Company. Batches of AlH_3 containing up to 1% Mg ion impurities was also used in this study. The intentional impurity Mg was present since it was believed that this ion would increase the thermal stability of the AlH_3. The reasoning behind this is somewhat analogous to the data which shows that multivalent cations can increase the thermal stability of nitronium perchlorate.(10) Both materials were stored in a dry box and, in general, exposed to the atmosphere as little as possible, in spite of the fact that the material reacted very slowly with water and was virtually unaffected by a 10 minute exposure to O_2 at 110°C. Chemical analyses of both the pure and Mg-doped AlH_3 are presented in Table 1. This same Table has been used to compare the thermal stability, expressed as 1% decomposition at 60°C, of these different samples.

TABLE 1

(C) Analysis Report of Mg Doped AlH_3*

Lot Nc.	Bulk Dens. (g/cc)	% Al	% Cl	% Li	% C	% H	% 1451	Days to 1% at 60°	% Mg
06276	0.75	88.5	0.01	0.12	0.07	9.96	95+	22	1.35
06286	0.75	87.8	0.01	0.16	0.17	10.00	100	17	0.90
07216	0.81	87.4	0.13	0.19	0.12	10.04	95+	13	1.40
11014A	0.79	89.8	< 0.10	0.12	0.10	10.05	95+		NONE

*All material is Mg-doped, but not treated with diphenyl acetylene (DPA).

1.2.2. Electrical Conductance

(U) Electrical conductivity measurements were made on pressed pellets made under vacuum, at a total force of 50 tons/in^2. The pellets were 1.25 cm in diameter and about .08 cm thick. It was found to be necessary to grind the AlH_3 (final particle size less than 44 μ) in order to form pellets which did not excessively flake. The front and rear surfaces were partially painted with Dupont silver conductive paint. Conductance measurements were made in a cell through which passed helium which had been passed over hot copper and through a liquid nitrogen cooled trap. The electrical circuit for these measurements is shown in Figure 1. Resistance measurements were taken with a Cary Model 32 vibrating reed electrometer equipped with a multiple resistor turret head. Voltages used were in the 0 to 40 V range (fields up to 500 V/cm). The voltage was only briefly applied to the pellet when taking readings, otherwise the pellet was shorted out. The temperature was measured with a thermocouple located in the gas stream near the pellet. Resistance measurements were taken at ascending temperature. Since the conductivity vs. reciprocal temperature plots were virtually identical for data taken either while the temperature was rapidly increasing or after the thermocouple had maintained a steady output for 10 minutes it is certain that the temperature indicated by the thermocouple must have been very close to the pellet temperature. Ohm's Law was found to be obeyed by the pellets, indicating that polarization effects were not important. The only geometric variable which affected the measured resistance was the electrode area pellet thickness ratio, thereby indicating that surface conduction was not of consequence.

(U)

Figure 1 Circuit diagram for electrical conductance measurements of AlH_3.

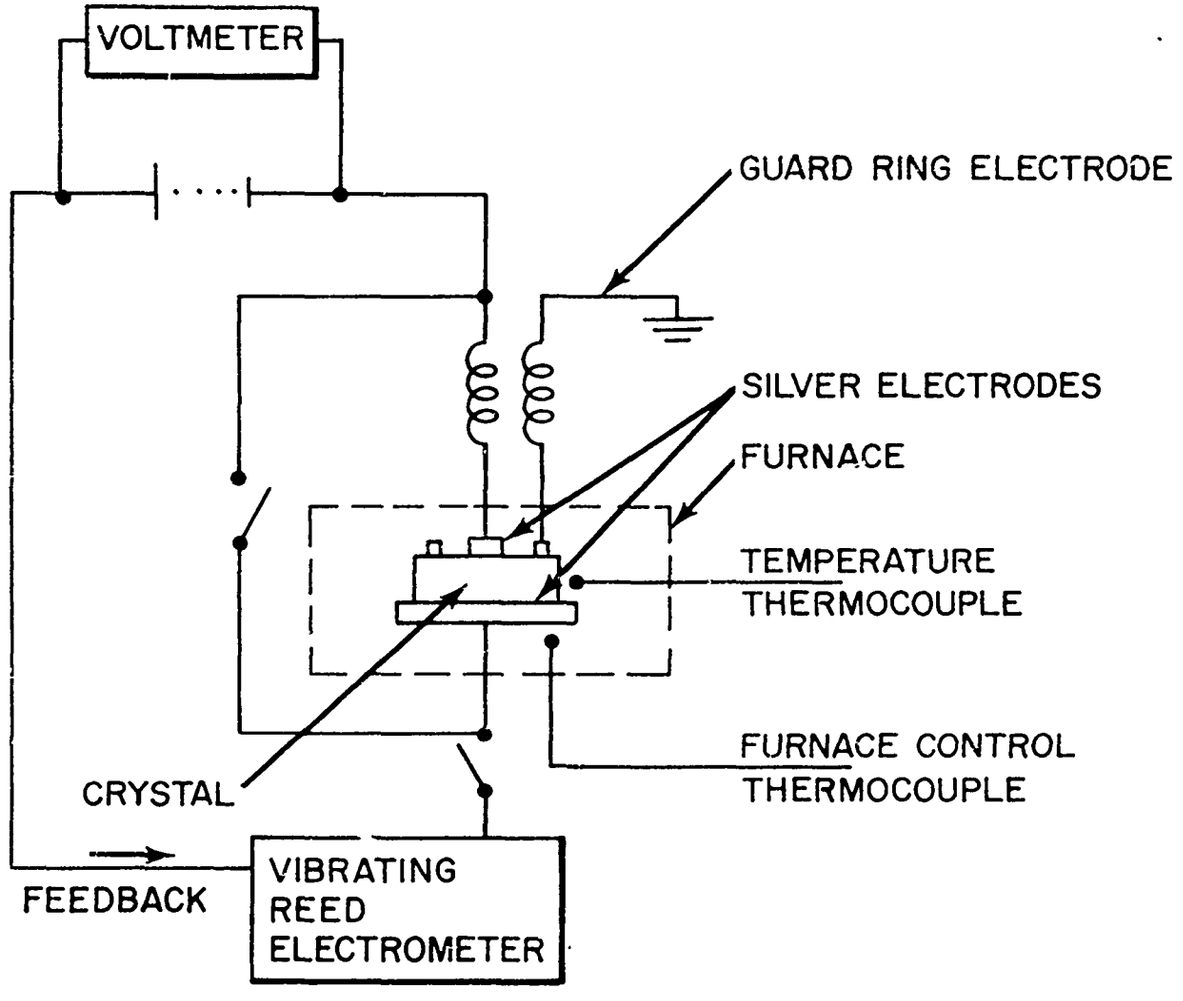
VOLTMETER
GUARD RING ELECTRODE
SILVER ELECTRODES
FURNACE
TEMPERATURE
THERMOCOUPLE
FURNACE CONTROL
THERMOCOUPLE
CRYSTAL
FEEDBACK
VIBRATING
REED
ELECTROMETER

Fig. 1

1.2.3. Thermal Analysis.

(U) Thermal decompositions were carried out in the temperature range 130 to 170°C in a conventional vacuum system, most of whose volume was contained in two traps which were immersed in liquid nitrogen, Figure 2. A Baratron gauge was used to follow the pressure. The DTA-TGA work was done on a Mettler vacuum recording thermoanalyzer. Platinum crucibles (diameter of 3 mm and height of 4 mm) were used to hold the 5-mg samples which had been vibrated. In the DTA the platinum cup which held the sample crucible served as one junction of the differential thermocouple; the other junction was the platinum cup which held the crucible with Al_2O_3 reference material. The oven temperature was measured at a platinum ring which encircled the crucibles, Figure 3. All runs were made in helium which was flowing past the sample at 10 l./hr. With a standard drying line (H_2SO_4, KOH pellets, and P_2O_5) it was found that the samples increased in weight during a run, presumably because of the presence of oxygen in the helium. This problem was eliminated by passing the helium through a tube filled with copper turnings at 440°C then through a liquid nitrogen trap. On the TGA runs, vibrated 25-mg samples in a platinum crucible (diameter of 8mm and height of 19mm) were used.

(U)
Figure 2 Block diagram of the all glass thermal decomposition line for AlH_3. A is the mechanical pump, B a 3 stage silicone oil diffusion pump, C an ionization gauge, D an alphatron gauge, E a Baratron gauge, F a thermocouple gauge, G an electrically heated oil bath. The volume between point X and the sample is 6.5 liters, Y and the sample 131cc.

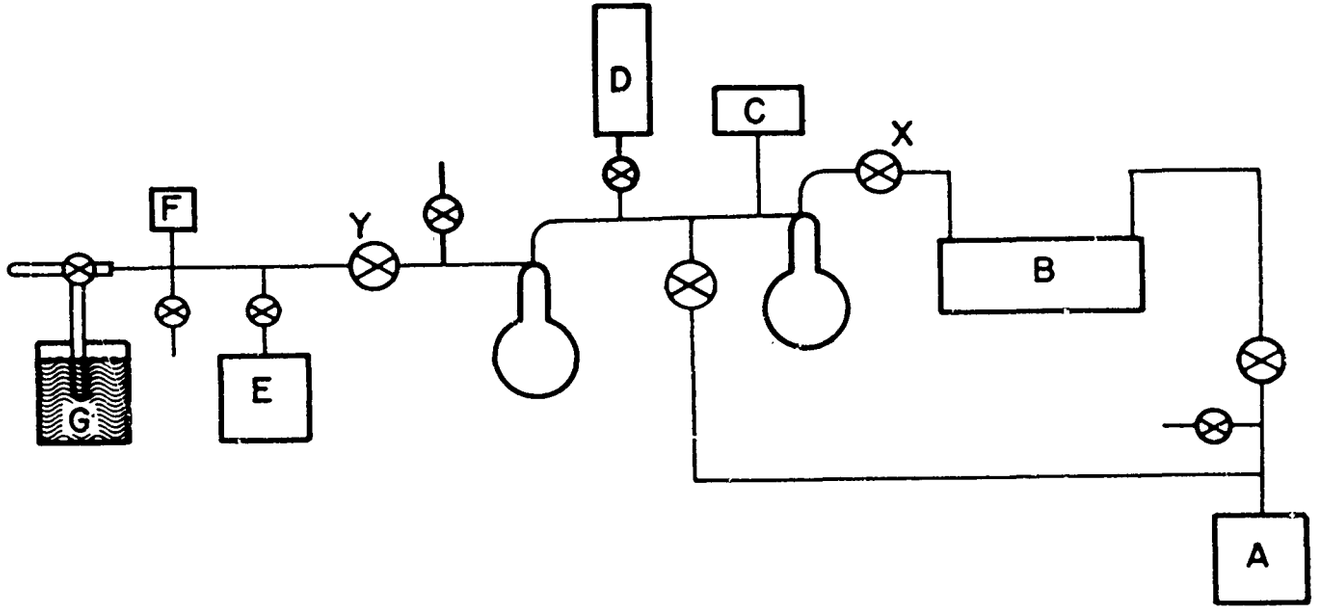

Fig. 2

(U)
Figure 3. Differential thermal analysis head assembly for the Mettler thermoanalyzer.

Fig. 3

1.3 Results (U)

1.3.1. Thermal Analysis - Kinetics.

(C) With the expectation that DTA could be used to characterize the thermal stability of AlH_3, samples from each of the three lots of Mg doped AlH_3 were subjected to simultaneous DTA/TGA. With 15 to 20 mg samples at a heating rate of 6°C/min only a single endotherm was found. Associated with the endotherm was a weight loss corresponding to total dehydrogenation of the sample, Figure 4. The temperatures at the minima in the endotherms of the three Mg-doped lots were 186°C, 190°C and 192°C for material whose stability expressed in days to 1% decomposition at 60°C were 10, 17 and 22 days respectively. These data imply that only a qualitative interpretation can be placed on DTA-thermal stability comparisons. That the DTA peak should correspond to an endotherm is consistent with the thermodynamic data on AlH_3[9] which, on extrapolation to the temperature where the endotherm occurs, indicate ΔH° for the decomposition should be positive. When oxygen and water are not rigorously excluded two partially resolved exotherms, Figure 5, were found instead of the single decomposition endotherm.

(C) Isothermal decompositions have been carried out on all four lots of pure and doped AlH_3 at several temperatures in the range 130 to 170°C. Upon analysis of these data it was found that a plot of $\ln t_{.01}$ vs $1/T$ (where $t_{.01}$ is the time necessary for 1% decomposition at T °K) is linear. Extrapolation of these plots to 60°C gave values of $t_{.01}$ which were comparable to but less than the values for the lots supplied with the material.

(U)

Figure 4. Simultaneous DTA-TGA of pure AlH_3 (20 mg) using calcined Al_2O_3 as the reference. Heating rate of $6^{\circ}C\ min^{-1}$ with the sample in a flowing O_2 free He atmosphere (10 liter $hour^{-1}$).

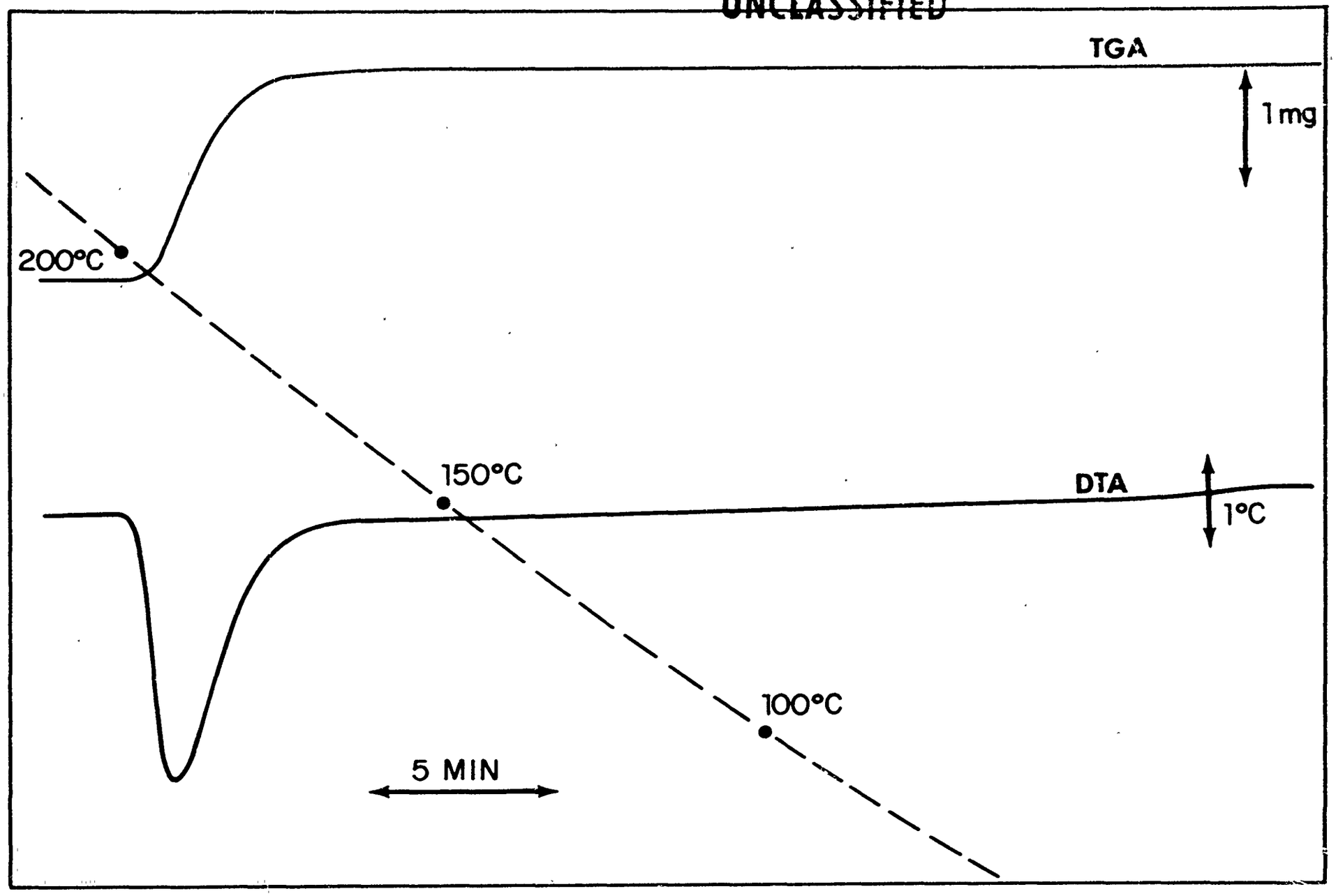

Fig. 4

(U)

Figure 5. Simultaneous DTA-TGA of pure AlH_3 (10 mg) using calcined Al_2O_3 as the reference. Heating rate of $6^{\circ}C\ min^{-1}$ with the sample in a flowing (10 liter $hour^{-1}$) atmosphere of He where no effort was made to remove O_2.

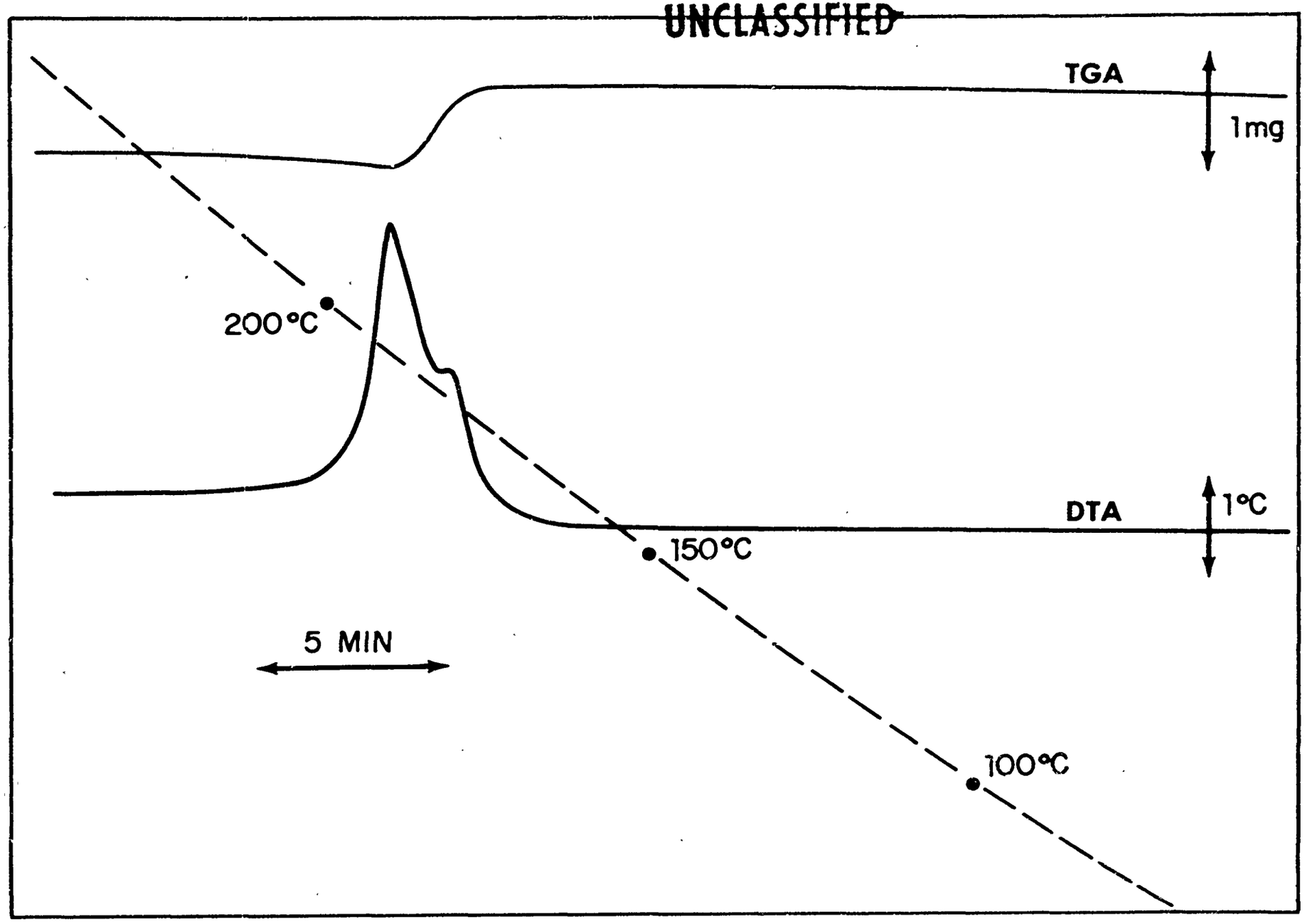

Fig. 5

Since the rate of decomposition is known to increase initially with the fraction of material decomposed it is likely that the extrapolated times are close to the correct $t_{.01}$ times. These same data have also been analyzed by the Prout-Tompkins equation:

$$kT = \ln \frac{(P + P_o) P_\infty}{(P_\infty - P) P_o} \qquad (1)$$

where P_o is a constant which must be determined for each run. It was found that for a given lot a plot of P_o/P_∞ vs. $1/T$ is linear with a negative slope. Rate constant values for AlH_3 analyzed by this technique are presented in Table 2.

(U) This expression fits the experimental P, t data very well for decompositions greater than 10%. An effort has been made to determine what kinetic processes are taking place in the first few percent of the decomposition. These efforts have resulted in a theory which adequately correlates the entire decomposition curve. It was noted that for small fractional decomposition, α, that α is proportional to t^n where n was generally 4 or occassionally a little less. Such a behavior for small α is predicted by a theory developed by Tompkins and others.[11] This theory discussed in detail in reference (11) is based on the hypothesis of a first order creation of random sites which can serve as growth centers (nuclei) for the decomposition. Assuming that once formed these centers linearly grow in three dimensions and accounting for coalescence of the centers as they grow the following is predicted:

$$-\ln(1-\alpha) = A \frac{k_2^3}{k_1^3} [\exp(-k_1 t) - 1 + k_1 t - (k_1 t)^2/2 + (k_1 t)^3/6] \qquad (2)$$

TABLE 2

Rate Constants for The Thermal Decomposition of Pure and Mg-doped AlH_3 (C)

RUN	LOT	T°C	$t_{.01}$(min)	k(min^{-1})	REMARKS
100	6276	133.5	133.5	-	Electrical furnace technique
101		168.5	5.15	0.330	
102		141.25	62.3	0.020	
103		151.75	24	0.073	
104		161.75	8.2	0.119	
105		177	-	0.381	
106		180.25	4.6	0.551	
109	6286	181	2.4	0.749	
110		141.3	21.4	0.013	
111		152.8	8.9	0.079	
112		164.5	5.05	0.239	
113		143.3	11.1	0.048	Used oil bath which gave better temperature regulation.
114	7216	161.7	3.8	0.39	
115		151.4	6.4	0.149	
116		143.4	10.3	0.062	
117		171	2.6	0.65	
118	7216	161.2	2.4	0.37	No N_2 in traps
119A		144.1	7.1	0.058	Preheated at 107°C for 2 1/2 minutes
120		120.7	52.3	-	

TABLE 2 (contd)

RUN	LOT	T°C	$t_{.01}$(min)	k(min^{-1})	REMARKS
121B		161.5	3.7	0.34	Preheated in O_2
122B		162.0	2.5	0.36	Preheated at 120° in NO_2 for 10 minutes
123B		162	2.8	0.37	Exposed to nitrobenzene vapor for 10 minutes at 120°
124	11014	151.7	4.4	0.34	
125		143.7	5.5	0.22	
126		170.9	2.0	0.99	
127		162	2.8	0.63	
128B		151.2	3.3	0.35	Treated with Nitrobenzene vapor
129B		151.5	3.9	0.35	Treated with O_2 10 min at 120°C
130B		151.6	3.4	0.34	Treated with NO_2 10 min at 120°C
131B		151.6	3.2	0.36	Treated with O_2 22 min at 120°C
132		151.5	(4.9)	0.37	Treated with diethyl ether for 10 min at room temp.
133		151.6	3.2	0.35	Kept under 19 Torr of O_2 for 64.5 hours at 60°C
134		151.7	5.2	0.32	Soaked in Tetrahydrofuran for 15 minutes at room temp.
135		151.7	4.3	0.34	Soaked in diethyl ether for 78 hours
136		151.7	5.0	0.35	Material ground-particle size 100-200 μ
137	7216	161.9	3.6	0.30	Soaked in tetrahydrofuran 10 minutes

TABLE 2 (contd)

RUN	LOT	T°C	$t_{.01}$(min)	k(min^{-1})	REMARKS
145	11014	151.8	4.9	0.34	Soaked in tetrahydrofuran 10 minutes
146	11014	151.8	5.1	0.31	Soaked in nitrobenzene 15 min.
147	11014	151.8	5.1	0.33	
148B	11014	151.8	4.3	0.34	Treated with water vapor at 120°C for 7 min.
151	7216	151.6	6.3	0.156	
153	5316	166.2	2.5	0.48	
154	5316	166.2	4.2	0.44	Soaked at pH 7 for 30 min.
155	5316	166.2	5.3	0.23	Soaked at pH 7 for 9 days
156	5316	166.2	4.6	0.35	Soaked 18 days in NBA
157	8176	166.2	2.2	0.49	
158	8176	166.4	4.0	0.45	Soaked at pH 7 for 30 min
159	8176	166.2	5.1	0.32	Soaked at pH 7 for 9 days
160	8176	166.2	(4.5)	0.42	Soaked 18 days in NBA
161	7216	166.1	3.3	-	No Traps
162	7216	151.4	6.0	-	No Traps
163	7216	124.8	38.3	-	
166	11014	166.8	2.5	0.79	
167	11014	156.7	4.0	0.47	
168	11014	137.0	11.1	0.13	
169	11014	131.2	13.9	0.074	
174	11014	156	5.2	0.55	No Traps
175	11014	152	4.2	0.38	Treated at 93°C to CO_2 for 20 min

where k_1 is the rate constant for the nuclei creation, k_2 is the rate constant for the nuclei growth and A is a constant for a given material. For small values of both α and $k_1 t$ this expression reduces to:

$$-\ln(1-\alpha) \approx \alpha \approx A\, k_2^3 k_1 t^4/24. \qquad (3)$$

(U) In the range $.1 \leq \alpha \leq .9$ Eq. 1 was satisfactory. Over a somewhat wider range of α Eq. 3 was also satisfactory, however, the value of the exponent varied with temperature being close to 4 at the highest temperature and near three at lower temperatures. A typical fractional decomposition (α) vs. time curve is shown in Figure 6 along with an analysis of this data by the Prout-Tompkins equation (1). For some runs equation (2) fit the data over a much wider value of α, Figure 7. At lower temperatures the fit was much poorer, even when corrections for the fact that α is not 0 at $t = 0$ were included.

(U) No systematic effort has been made to check the validity of the full expression for $-\ln(1-\alpha)$, however, for those cases which have been tried the fit is more than satisfactory. Figure 7 demonstrates this adequacy. The minor deviations from linearity are most likely caused by a somewhat improper value of k_1, the fact that it takes a while for the sample to come up to temperature, and since at $t = 0$, α is not zero.

(U) The ramifications of the success of this theory are worth considering. The initial t^4 dependency strongly suggests that the basic mechanism of the decomposition is not surface initiated.

(U)

Figure 6. A plot of possible analytical approaches to a thermal decomposition run of pure AlH_3 at 130°C. The sigmoid curve is a plot of the fractional decomposition, α, vs. time and the straight line a plot of $\ln [(\alpha + 0.0064)/1-\alpha] + 5$ vs. time.

UNCLASSIFIED

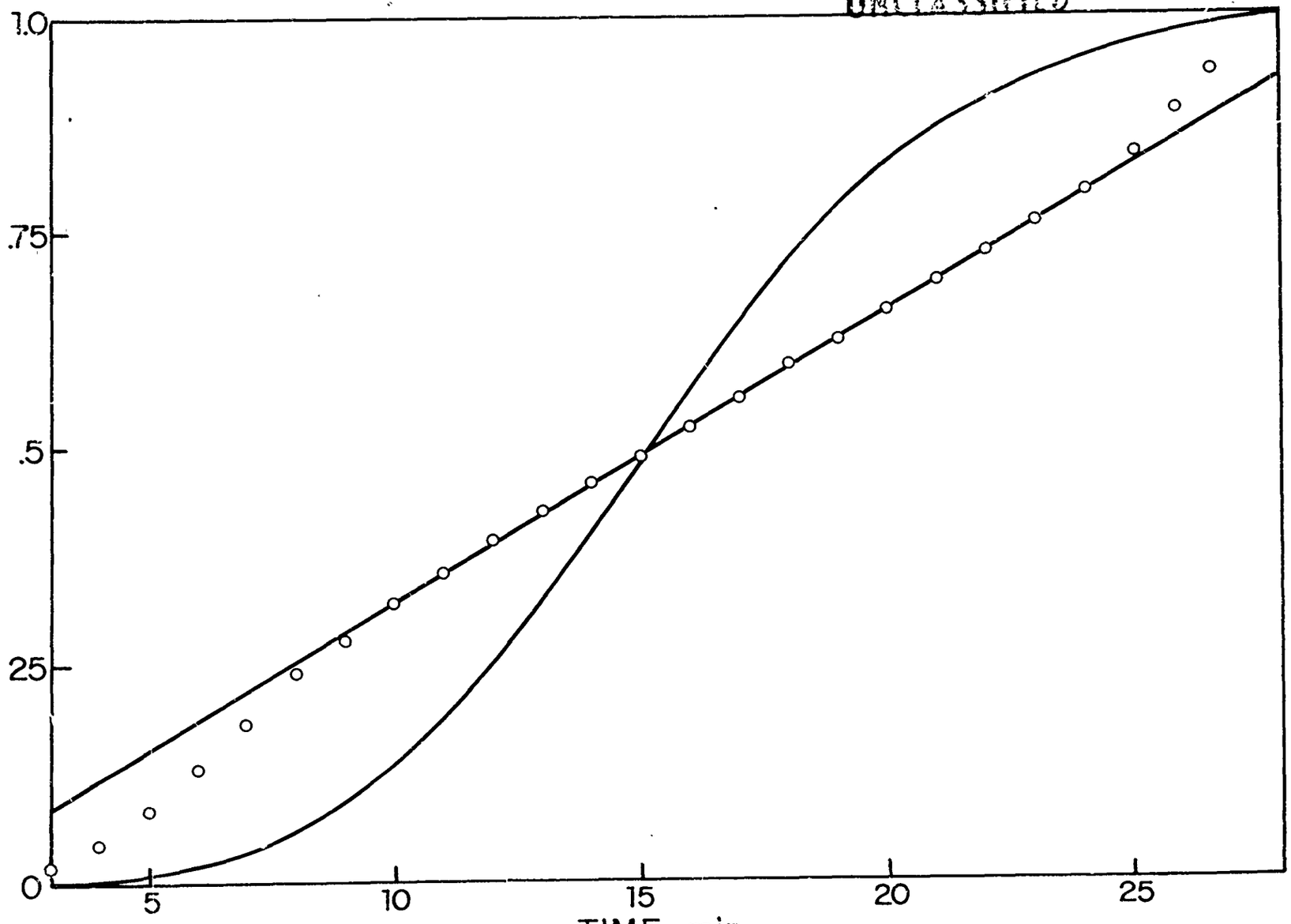

Fig. 6

UNCLASSIFIED

(U)

Figure 7. A further analytical approach to the thermal decomposition of AlH_3 at 130°C. This is plotted as $-\ln(1-\alpha)$ vs. S where

$S = e^{-\theta} - 1 + \theta + \frac{\theta^2}{2} + \frac{\theta^3}{6}$ where $\theta = k_1 t$.

UNCLASSIFIED

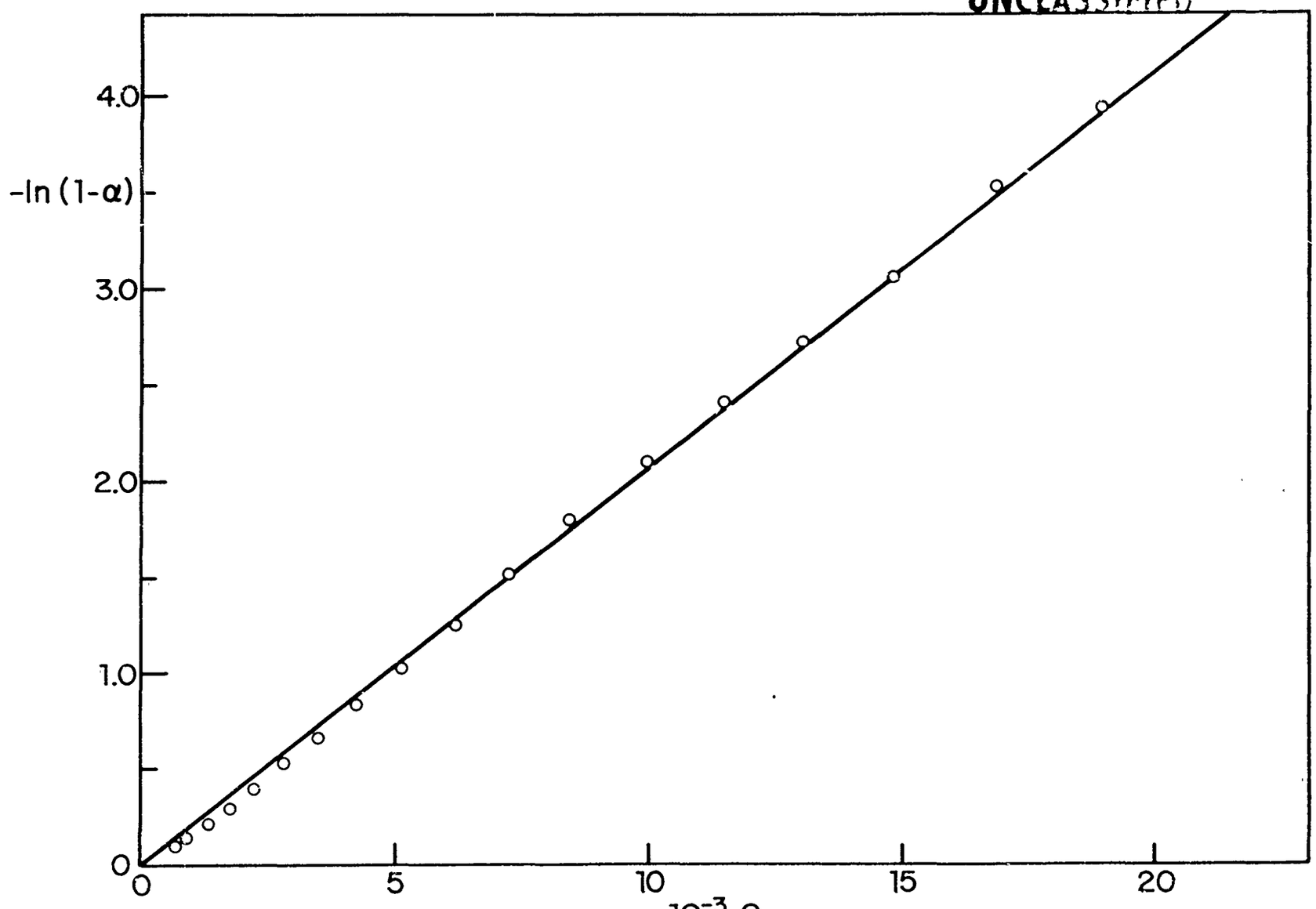

Fig. 7

UNCLASSIFIED

(C) The lack of satisfactory fit over the entire range in α for all temperatures employed suggests that none of the expressions, as applied to AlH_3, are of fundamental significance. To avoid employing physical significance where none exists, the data were treated following Jacobs and Kureishy,[12] i.e. ln $(t_{n'} - t_n)$ was plotted vs. 1/T where t_n is the time for α to reach n with the activation energy taken as R times the slope. The activation energy so determined was independent of n and n' provided they were in the range .1 to .9. The results for four samples are summarized in Table 3.

1.3.2. Thermal Analysis -Surface Treatment.

(C) On the basis of prior work it was suggested that the stability of AlH_3 may be a surface related phenomenon.[13] On the assumption that this hypothesis is correct, we have attempted to modify the AlH_3 surface by reacting AlH_3 with various foreign gases with the objective of increasing its stability. The general technique which has been followed is to expose a sample of AlH_3 at 120°C to a foreign gas for about 10 minutes followed by rapid thermal quenching and simultaneous pumping off of the gas. This procedure should result in little if any of the foreign gas being either physically adsorbed or weakly chemisorbed on the AlH_3. The following gases have been employed; O_2, Cl_2, NO, NO_2, NOCl, HCl, C_3H_4 (Allene), CO_2, and $C_6H_5NO_2$ (nitrobenzene). As a rule, the treatment does not lead to any significant change in k (as determined by rate data excluding the first 10% of decomposition). The treatment does change $t_{.01}$ as can be seen in Table 4. Improvements in stability were found for two lots of AlH_3 treated by Dow Chemical Co. by prolonged exposure to water buffered at pH 7 or to N-butylamine.

TABLE 3

(C) Comparison of the Thermal Decomposition Activation Energies for Pure and Mg-doped AlH_3

Sample	Mg%	Li%	Thermal Stability (days)	Activation Energy Decomposition* Kcal/mole	Conductivity at 100°C $(ohm\text{-}cm)^{-1}$
"Pure" AlH_3	0	0.12	4 1/2	20 ± 2	3.3×10^{-10}
M_3	1.4	0.19	13	30 ± 2	-
M_2	0.9	0.16	17	30 ± 2	3.6×10^{-11}
M_1	1.3_5	0.12	22	30 ± 2	1.8×10^{-11}

*Note the change in activation energy for the pure vs. doped samples.

TABLE 4

Effect on the Decomposition Kinetic Parameters of AlH_3 by Exposure to Various Gases

(U) Treatment	Lot 7216[a] $t_{.01}$(min)	Lot 7216[a] k(min)	Lot 11014[b] $t_{.01}$(min)	Lot 11014[b] k(min)
No treatment	3.8	0.39	4.4	0.34
			5.1	0.33
O_2 7 1/2 min 120°C	3.7	0.34		
O_2 10 min 120°C			3.9	0.35
O_2 22 min 120°C			3.2	0.36
O_2 64 hours 60°C			3.2	0.35
NO_2 10 min 120°C	2.5	0.36	3.4	0.34
$C_6H_5NO_2$ vapor 10 min 120°C	2.8	0.37	3.3	0.35
H_2O 7 min 120°C			4.3	0.34
Crushed 100-200 mesh			5.0	0.35
Tetrahydrofuran wash (15 min)	3.6	0.30	5.2	0.32
			4.9	0.34
Ether wash 15 min			4.9	0.37
Ether wash 78 hours			4.3	0.34
$C_6H_5NO_2$ wash 15 min			5.1	0.31
CO_2 20 min 93°C			4.2	0.38
	Lot 5316[c]		Lot 8176[c]	
No Treatment	2.5	0.48	2.2	0.49
Water at pH 7 for 30 min	4.2	0.44	4.0	0.45
Water at pH 7 for 9 days	5.3	0.23	5.1	0.32
N-Butyl amine for 18 days	4.6	0.35	4.5	0.42

[a] Measured at 162°C

[b] Measured at 152°C

[c] Measured at 166°C

For oxygen the exposure conditions were varied by exposing at 120°C for both 10 min. and 20 min. and at 60° for 64 hours. From these results it was concluded that there was no reason to believe that differing exposure conditions with the other gases would lead to any marked improvement.

(C) Table 4 also lists values of $t_{.01}$ for AlH_3 which had been washed in diethyly ether, tetrahydrofuran and nitrobenzene. While some improvements in $t_{.01}$ exist they are hardly significant.

1.3.3. Thermal Analysis - Mass Spectrometry.

(C) The initial mass spectrometric study was achieved by collecting some of the decomposition products in a closed vessel and then leaking these species into a conventional magnetic mass spectrometer (Consolidated Electrodynamics 21-613 residual gas analyzer). Mass spectra of the decomposition products from three lots of Mg doped AlH_3 and one undoped sample have been taken. Also four mass numbers have been gated on during a decomposition. The value of the former experiment is somewhat limited since it was later determined that the mass spectrometer was partially defocused. Since the effects of the defocusing increased with mass it was not possible to identify all the species present in the usual manner, i.e. comparing the observed fragmentation patterns to previously obtained fragmentation patterns of pure substances. Nonetheless we can confidently state that both ether and benzene plus other species were present. While this result is to be expected, the pressure-time evolution was somewhat surprising. These can be seen in Fig. 8. From these curves it seems clear

(U)

Figure 8. Relationship between mass spectrometrically determined decomposition species and time for "pure" AlH_3. The species $(C_2H_5)_2O$ and C_6H_6 are due to occlusions of these solvents used in the preparation of AlH_3.

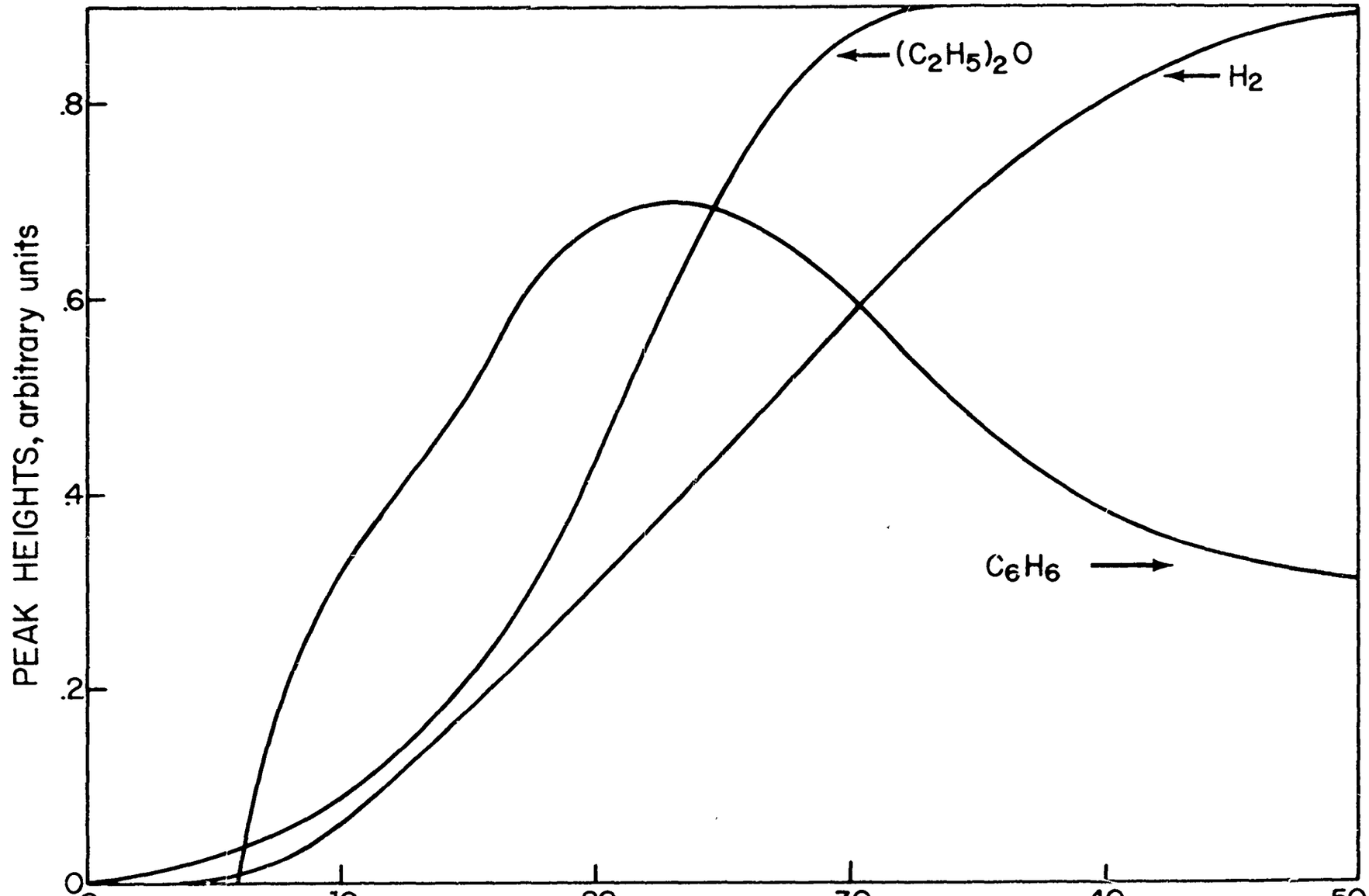
$(C_2H_5)_2O$
H_2
C_6H_6
PEAK HEIGHTS, arbitrary units
0
.2
.4
.6
.8
0
10
20
30
40
50
TIME, min.

Fig. 8

that both benzene and ether are dispersed in the crystals and are not merely absorbed on the surface. The reason for the decrease in the benzene peak is not clear. It is most unlikely that the decrease results from catalytic reduction of benzene on the Al surface at the temperature of the run, 150°C. Figure 9 shows the relative growth of mass peaks 44 and 43. Both of these peaks were very prominent, however, it was not possible to definitely determine what species they resulted from.

(U) Table 5 shows that there appears to be some correlation with stability and the relative intensities of several of the mass peaks. Whether this correlation is of fundamental significance is impossible to state. The same situation also holds for other correlations which have been suggested.

TABLE 5

Relationship Between the Thermal Stability (Days to 1% Decomposition at 60°C) and The Intensity of The m/e Peaks (C)

Days at 60° to 1% Decomposition =	4 1/2 (Not Doped)	13 (Mg Doped)	17 (Mg Doped)	22 (Mg Doped)
m/e = 15	35	80	120	140
m/e = 44	50	130	150	160
m/e = 45	65	145	180	190
m/e = 58	11	40	40	45
m/e = 59	16	50	50	55

(U)

Figure 9. Relationship between two unassigned mass numbers, 44 and 43 and time for decomposing AlH_3. These data, as also those of Figure 8, are obtained by continuous gating with a Bendix T.O.F. mass spectrometer.

UNCLASSIFIED

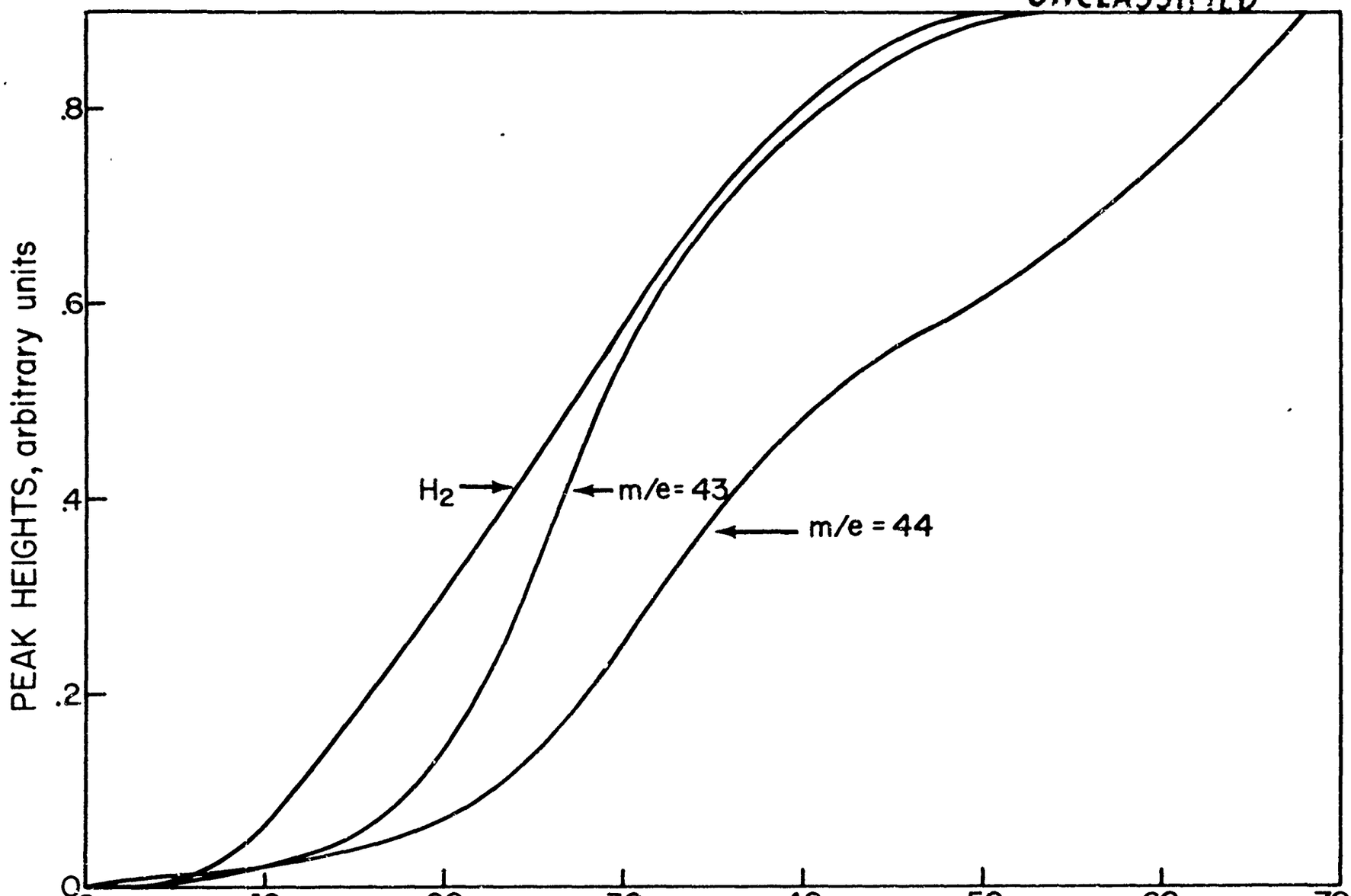

Fig. 9

UNCLASSIFIED

(U) A Bendix time-of-flight mass spectrometer has been used for further substantiation of the earlier mass spectrometric conclusions. Because it could be performed so conveniently the decomposition of two lots of AlH_3 were followed on the TOF. The samples were run in the heated crucible sample inlet system at about 180°C. Because of the high pumping speed of the system and because of the closeness of the sample to the ionizing beam, the signal from the mass spectrometer for any ion is proportional to the rate of formation of the "parent" of the ion. This differs from the work reported earlier in which the decomposition products formed in a closed system were leaked into a single mass spectrometer. The principle advantages of the time-of-flight system is that five mass peaks can be monitored simultaneously and that the products detected could not have resulted from secondary reactions.

(C) The results of the TOF runs are generally consistent with the results reported earlier. Mass peaks 43 ($C_3H_7^+$ possibly from acetone), 44 (CO_2^+ ?), 45 ($C_2H_5O^+$ from ether), 2 (H_2^+) and 78 ($C_6H_6^+$) have been monitored. The samples were decomposed at 180°C. When the heat was turned on the signal for mass peaks 43, 44, 45 and possibly 78 rose and then fell. The source of these maxima are most likely out gassing of species adsorbed on the surface. The mass signals for masses 43 and 45 closely paralleled each other with their maxima coming before that of H_2. Likewise the maximum in the mass 44 peak and the 78 peak also came before the H_2 maximum, with the 78 peak being the earliest. From this work we can conclude that the species observed are present within the bulk of the AlH_3 crystal and are not merely adsorbed on the surface. On the basis of the information we have on the manufacture of AlH_3 the presence of the mass peaks 44 and 43 still remains a mystery.

1.3.4. Effects of Light on AlH_3.

(C) Initially only slight precautions were taken to avoid exposing the AlH_3 samples to light. Were the samples white, exposure to normal room light would not be expected to have any effect. However, since all the samples were varying shades of grey (indicating the possibility of light absorptivity throughout the entire visible range) a test of the photosensitivity was indicated. Tests were made on samples placed in a rotating quartz tube in an atmosphere of flowing He. A low pressure mercury arc was situated about 2 cm from the top of the 2.5 cm o.d. tube. Without a filter the predominant wavelength emitted by the lamp is 2537Å. In the experiments with filters only light of wavelength greater than about 2800Å was passed. The results of these experiments are summarized in Table 6. It is clear that light does affect the stability of AlH_3, with the effect being most pronounced at the beginning of the photolysis. Further, the exposed samples seem to partially recover their initial stability on storing for a few days. Material which has been exposed to light changes color, becoming darker, and is far more reactive with water than the unexposed samples. The 0-53 filter, which is simply untreated pyrex glass, eliminates the strong 2537Å line and reduces the total intensity by a factor of over two. Even with the reduced intensity and longer wavelength employed, the reduced stability was evident. However, the weakest intensity used in the photolyses was about 100 times greater than normal laboratory light intensity so that other than avoiding long term exposure to room light no other precautions are indicated.

TABLE 6

(U) Effect of U.V. - Visible Photon Irradiation on AlH_3

(C) Run	Light Exposure Time	Conditions	$k(min^{-1})^*$	$t_{.01}(min)^{**}$
150A	30 min	No filter	0.345	4.40
150B	2 hours	No filter	0.390	3.22
150C	2 hours	Same as 150B except tested 4 days later	0.369	4.03
151	0 hours	Starting material	0.156	6.26
152A	2 hours	Corning 0-53 filter	0.307	4.80
152B	2 hours one day + 2 hours next day	Corning 0-53 filter	0.335	5.20

*Temp. = 152°C, k determined by $1.1/(t_{1/2} - t_{1/4})$.

**$t_{0.01}$ = time at 152°C for 1% decomposition.

1.3.5. Electrical Conductance of AlH_3.

(C) Plots of the logarithm of the electrical conductance against reciprocal temperature for pure AlH_3 and two of the Mg-doped AlH_3 pressed pellets are shown in Figure 10. These data are extremely reproducible. Samples showed excellent Ohm's Law dependance at all temperatures, indicating the absence of any space charge formation during the conductance experiments. The results of the conductivity vs. temperature data are also summarized in Table 3, (see also Fig. 10). Isothermal experiments carried out at temperatures where decomposition was taking place showed that the conductivity was a weak monotomic increasing function of time up to about $\alpha = .5$ (see Fig. 11). At that point the conductivity increased several orders of magnitude suggesting that a metallic conduction path existed.

(U)

Figure 10. Plot of the electrical conductance, σ, as a function of temperature for pure and doped AlH_3.

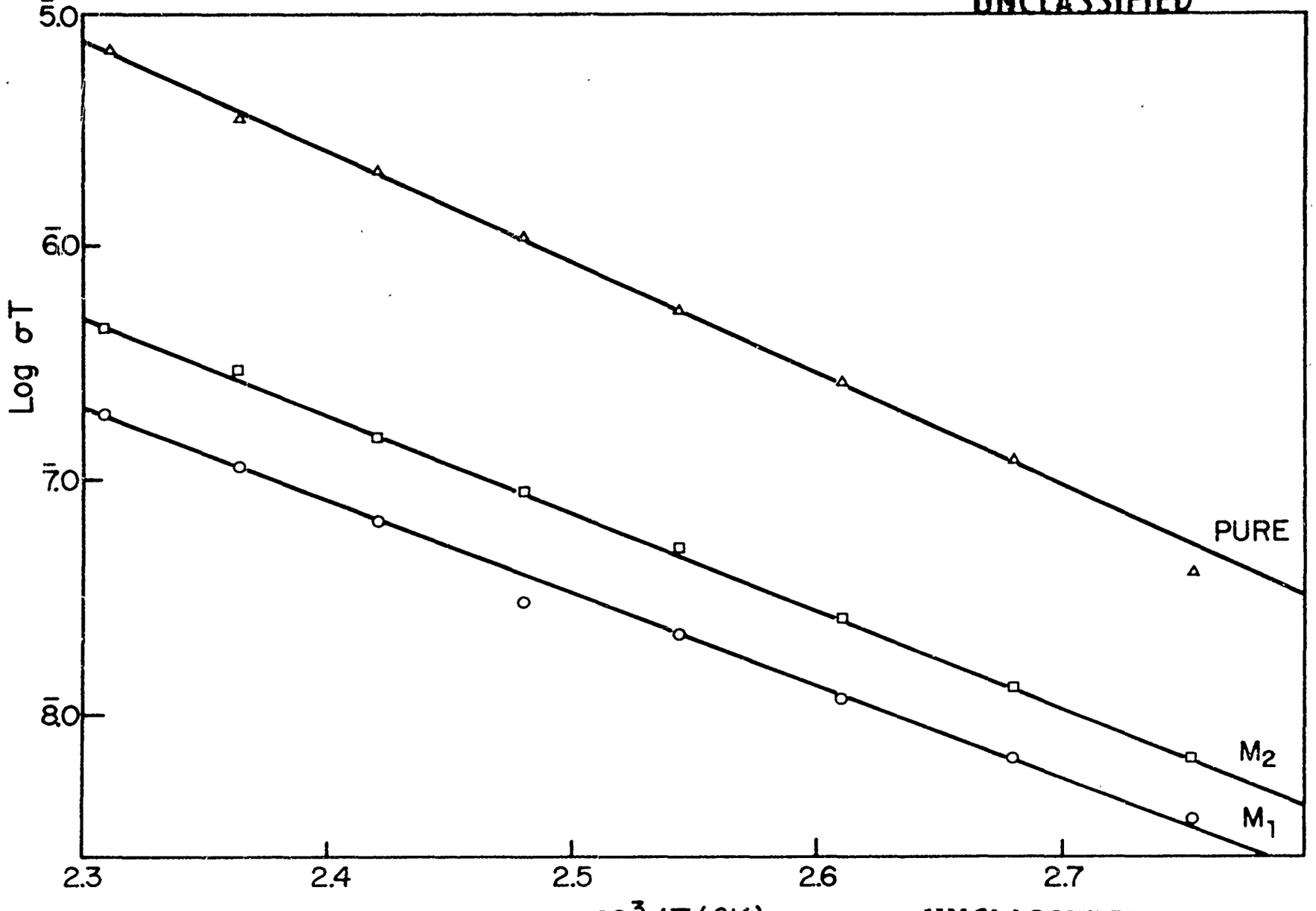

Fig. 10

(U)

Figure 11. Relationship between the electrical conductance, σ, and time for AlH_3 hold isothermally at 120°C.

UNCLASSIFIED

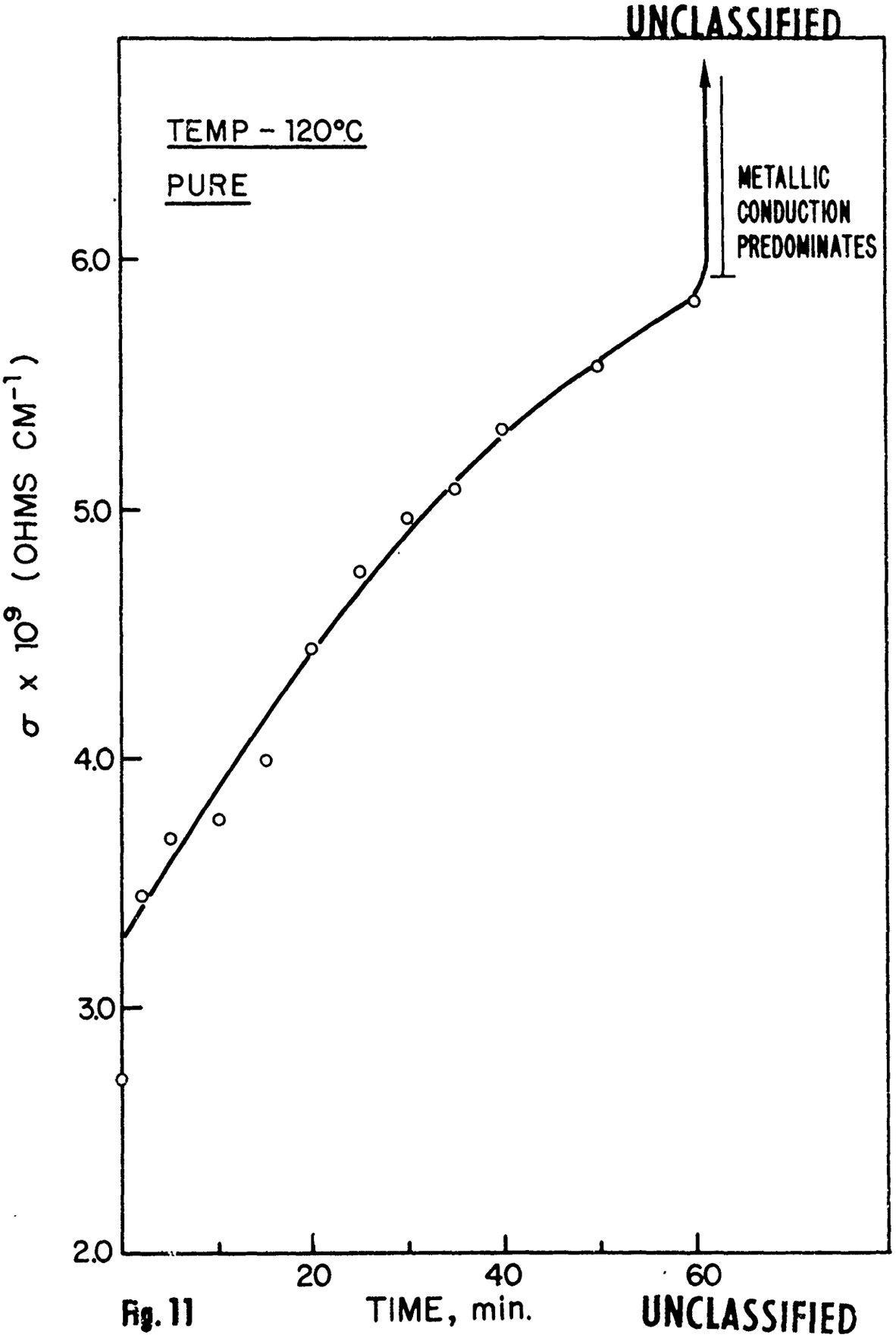

Fig. 11

UNCLASSIFIED

1.4. Discussion (C)

(C) Interpretation of the conductance data of Figure 10 is complicated by the absence of any "knee". The activation energy associated with this conductance data is 0.9 ev, and is concluded to be due to either electronic or ionic conductance. Generally an electrical conductance vs. temperature plot is composed of two straight lines of different slopes joined together at a "knee". These two lines are referred to as the extrinsic and intrinsic conduction lines. The intrinsic data is that conductance data which is determined solely by the temperature of the sample and is reproducible from sample to sample and also reproducible from investigator to investigator. In comparison the extrinsic data is determined primarily by the unintentional impurities present in the sample such that these data vary with the history of the sample. For an electronic conductor the slope of the intrinsic curve is approximately twice that of the extrinsic data. If our data is extrinsic the activation energy for intrinsic conductance would be 1.8 ev. These values of 0.9 and 1.8 ev should correspond qualitatively to the optical absorption energy of AlH_3 thus predicting that AlH_3 should be blue or metallic in color. However, AlH_3 is colorless, implying that its optical absorption energy is greater than 3 ev. It is reasonable to conclude, therefore, that the conductance being measured is not due to electronic carriers.

(C) A possible alternative is ionic conduction. Since the ionic radii of Al^{3+} and H^- are ~ 0.5 Å and ~ 1.5 Å, respectively, the Al^{3+} ion would probably be the charge carrying species due to its smaller size. Assuming this to be the case the activation energy of 0.9 ev must be an extrinsic

value since intrinsic values are always observed to fall at about 2.0 ev. A theoretical interpretation of ionic conductance shows that the cation conductance (intrinsic) is given by:

$$\sigma T = (4e^2a^2N\gamma/k)\exp\ (\Delta S_1 + \frac{s}{2})/k\ \exp\ -(\Delta h_1 + \frac{h}{2})/kT$$

where Δh_1 is the enthalpy of migration, h the enthalpy of defect formation, ΔS_1 and S the entropy values of these processes, γ the lattice vibrational frequency of an ion adjacent to a vacancy. Conductance below the "knee" will be extrinsic and dependent only on the number of vacancies produced by the unintentional impurities such that the slope will be equivalent to $\Delta h_1/2.303k$. Using this analytical model we find that $\Delta h_1 = 0.9$ ev. Using this model, incorporation of Mg^{2+} substitutionally into the AlH_3 lattice requires that the number of cation vacancies (i.e. charge carriers) be decreased with a resultant depression of the electrical conductance. This is evident in Figure 10 for M_2 (0.9 mole % Mg) and M_1 (1.4 Mole % Mg). These data help to substantiate the ionic conductivity model of cation charge carriers.

(C) The trend of $M_1 > M_2$ in conductance depression is correct but the magnitude of the depression is too small. With these levels of assumed substitutional doping the conductance should have been depressed to about 10^{-10} ohm cm^{-1}. From a knowledge of other doped systems it is possible that all the Mg does not enter the lattice substitutionally. If this is true then the conductance depression would be small and comparable to that observed. The Mg that does not enter substitutionally will separate out as a second phase, possibly as magnesium hydride or magnesium aluminum hydride.

(C) The important features of the thermal and electrical studies are 1) the different thermal decomposition activation energies for pure and doped AlH_3, 2) t^4 dependence of the fractional decomposition, 3) depression of electrical conductivity by 'substitutional' Mg, 4) apparent second phase separation and 5) independence from sample geometry of the electrical conductance, thus excluding the possibility of surface conduction.

(C) If, as is probable from the conductance data, a second phase separates out in the Mg-doped AlH_3, it will do so at kink sites (Fig. 12, point c), ledge sites or at other gross imperfection sites since these are thermodynamically most favorable. The difference in thermal activation energies for pure and doped AlH_3 can then be explained with this model. The H_2 formed in the decomposition of AlH_3 will tend to leave the crystal at some site such as b or c, but not in the plane, a. If in the doped material the preferential sites b and c are not occupied by AlH_3 then the H_2 must leave from a higher energy site. The fact that x-ray analysis (Dow Chemical Co.) has not revealed any impurity hydride is not surprising due to its low concentration and small crystalite size.

(C) The passivating effect of surface coatings on AlH_3 as demonstrated by Dow may also be explained by this model since sites such as d are favored in any absorption processes thus tending to lower the activity of sites b and c in Figure 12.

(U)

Figure 12. An idealized diagram showing a possible configuration for the surface of AlH_3. From this figure point d would be the point of highest chemical activity.

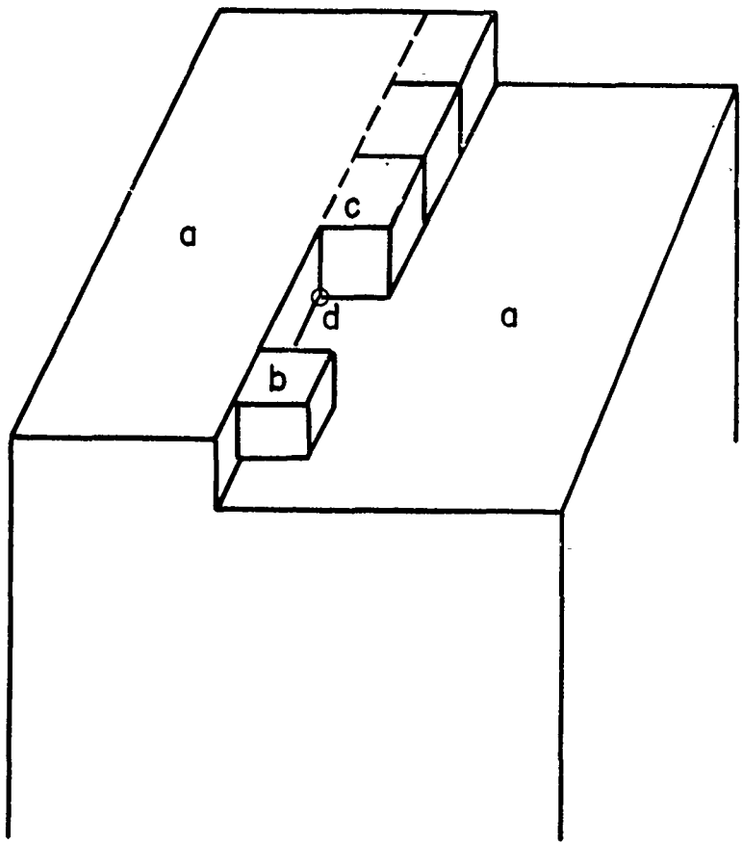

Fig. 12

(C) All available samples of AlH_3 had as an impurity Li, in about 0.1 weight percent. Since changes in the decomposition rate of pure AlH_3 substitutionally doped with either Li or Mg should be in the same direction (i.e. faster or slower) and of comparable magnitude and since the concentrations of Li in the samples are greater than is necessary to produce marked changes in the decomposition rates of other materials there is greater reason to believe that the effect of Mg is through the proposed surface mechanism. It is worth while noting that the presence of singly or doubly charged positive ions may actually increase the rate of decomposition relative to pure AlH_3. In this case doping with tetrapositive ions would decrease the rate.

1.5. Conclusions and Recommendations.

(C) If the preceding model is correct, the Mg-doped AlH_3 shows improved stability due to elimination of active sites; the extent of substitutional doping is negligible and perhaps even speeds up the decomposition. The presence (unintentional) of Li also contributes. The difficulty in manufacturing AlH_3 of consistent quality is probably connected with the nature of this second phase formation.

(C) From these data and the proposed stability model it is our opinion that true substitutional atomic doping will not work with AlH_3 until it can be repeatedly prepared in the pure state, e.g. without any unintentional impurities such as the high concentrations of non-substitutional Li presently found.

(U) Other stabilization techniques which are being considered include encapsulation. Our opinion is that this technique will provide only a passivation effect, but not the needed long term stability; since while surface coatings may suppress surface reaction they do not prevent hydrogen formation in the bulk of the material.

2. Solid State Chemistry of Hydroxylammonium Perchlorate (HAP) (U)

2.1. Introduction and Objective.(U)

(U) Hydroxylammonium perchlorate (HAP) is a white, granular, hygroscopic solid whose thermogram indicates an endothermic transformation at 55-60°C, melting endotherm at 85-90°C and its decomposition exotherm at 240-250°C. Three crystalline phases of HAP have been examined by Dickens[14] using the x-ray diffraction technique. The crystal structure of the most stable phase was determined as orthorhombic having a space group of $P2_1cn$ and cell dimensions of 7.52, 7.14 and 15.99 Å at 25°C. The general structure is considered to consist of chains of perchlorate ion tetrahedra held together by hydrogen bonding from parallel chains of NH_3OH^+ ions. A complete presentation of the various crystal phases of HAP is given in Figure 13.

(U) The presently held model for the thermal decomposition of HAP with small heating rates[15] indicates that the initial step in the decomposition involves dissociation of the salt to free amine and perchloric acid. This reaction is then followed by the oxidation and decomposition of hydroxylamine and perchloric acid to give a multitude of side products including AP and O_2. The dissociation step has been verified by direct inlet mass spectrometric studies at the Rocket Propulsion Laboratory. By the relative intensity peak height technique (for NH_2OH) an activation energy of 20 kcal $mole^{-1}$ has been calculated for the formation of NH_2OH and $HClO_4$. However, a break in the activation energy slope was observed at 60°C with a lower E_a being observed above this temperature. Similarly compatability studies at the Midwest Research Institute have shown that the compatibility of HAP in a propellant system is reduced above the 55°C endotherm. The conclusions to be drawn from these data is that the 55°C endotherm is somehow responsible

(U)
Figure 13. Description of the various crystal phases of HAP determined primarily by the Navy Propellant Plant.[14]

CRYSTAL STRUCTURES OF HAP

PHASE A $\underset{\text{SLOWLY REVERSIBLE}}{\overset{60°C}{\rightleftharpoons}}$ PHASE B $\overset{90°C}{\rightleftharpoons}$ MELT $\underset{\text{57-58°C HEATING}}{\overset{\text{(~50% CHANCE) COOLING}}{\rightleftharpoons}}$ PHASE C

DENSITY (g/cm^3)	$\rho^{25°C} = 2.065 \pm 0.008$; $\rho^{23°C} = 2.051 \pm 0.019$		$\rho^{30°C} = 2.26$
CRYSTAL STRUCTURE	ORTHORHOMBIC	MONOCLINIC	MONOCLINIC
SPACE GROUP	$P2_1\,cn$	$P2_1/n$	C2/m, C2 or Cm
MOLECULES / UNIT CELL	8	12	16

Fig. 13

for an increase in the chemical reactivity at this temperature.

(U) The main objective of the present program is directed toward defining the nature of the first endotherm, phase change or dehydration. Also, the establishment of any relationship between the postulated dissociation mechanism and crystal behavior is relevant to this study.

2.2. Experimental Techniques. (U)

2.2.1. Materials and Thermal Analysis Testing (U)

(U) Two different batches of material were used. One batch was obtained from the Naval Propellant plant and is herein designated as Navy HAP. The other batch was from the Thiokol Chemical Corporation and is designated as Thiokol HAP. Thiokol HAP was received in dessicated bottles and was specified as being 98% minimum assay with a particle size range of 44 to 840 microns. The Navy HAP was received as a carbon tetrachloride slurry. Prior to testing, the Navy material was filtered through a Buchner funnel and then vacuum dried for 2 days with continuous pumping. An additional sample of Navy HAP was also received which had been packed dry rather than as a slurry with carbon tetrachloride.

(U) In tests involving DTA measurements, 15 mg of Al_2O_3 were weighed into a platinum cup (3 mm dia. x 5 mm ht.) and placed in the reference holder of the Mettler thermoanalyzer (see part 1 of this report). The thermoanalyzer was then pumped down to approximately 8×10^{-5} Torr with diffusion pumps and filled with dry helium. The HAP sample was then loaded into a similar cup inside the dry box with the amount of sample being determined volumetrically to give a weight of approximately 30 mg. Precise

weight determination was made gravimetrically after testing. The sample was transferred from the dry box to the thermoanalyzer in a closed container having a dry nitrogen atmosphere. Loading the sample into the thermoanalyzer was performed inside a large bell jar through which a high flow rate of helium was being maintained, Figure 14. A similar procedure was followed for tests involving only TGA measurements except that elimination of the need for reference material and differential thermocouple permitted the use of a 16 mm diameter platinum macro cup capable of holding up to 700 mg of sample. All thermal testing was performed on the most sensitive weight scale permitting detection of weight changes as small as one microgram. DTA sensitivity was either 2 or 10 microvolts per inch using a Pt vs. Pt-10% Rh thermocouple for which a differential temperature of 1° corresponds to about 7 microvolts over the temperature range of 50-100°C. A flow rate of 5 liters per hour was maintained during testing using helium which had been passed through H_2SO_4 and P_2O_5 drying towers and deoxygenated over hot copper. Estimates of enthalpy values are based upon measurements of DTA peak areas using a calibration factor derived from potassium nitrate melting and freezing peaks. No adjustment has been attempted for factors such as thermal conduction, specific heat, etc. which can influence peak size but are very difficult to evaluate.

(U)

Figure 14. Photograph of the Bell jar in use with the Mettler thermoanalyzer. This technique allows the loading of the DTA stick to be carried out in an inert atmosphere.

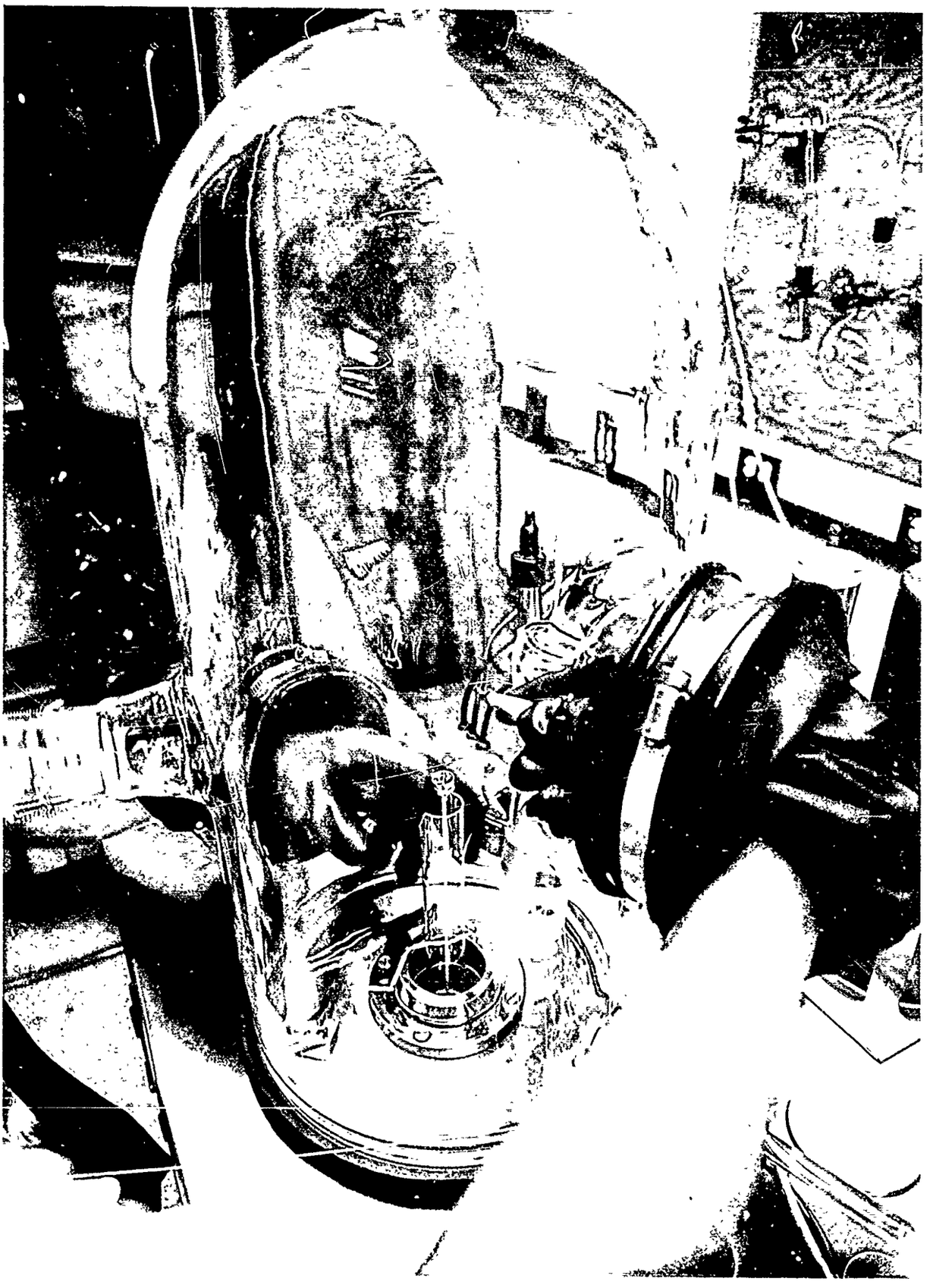

Fig. 14

2.2.2. Thermal Microscopy (U)

(U) Due to the nature of the problem being investigated, i.e. phase change or dehydration, it was felt worthwhile to attempt a thermal microscopy study of HAP upto its melting point. The equipment used was a Mettler FP2 programmed thermal microscope* completely enclosed in a dry bag containing dry helium, Figure 15. The attractive feature of the Mettler hot stage is that the sample under investigation is placed between two identical heating plates. This means that it is possible to measure temperatures accurately without imbedding a thermistor in the sample or calibrating a thermometer.

(U) A typical program involved preparing a uniform sample between a microscope slide and a cover glass, inserting the sample into the hot stage and selecting the appropriate thermal program for the study. With the instrument used it was possible to select heating and cooling rates between 10° and $0.2^{\circ}C\ min^{-1}$ and alsc to maintain isothermal conditions. To photographically record phenomena seen through the Nikon Model S-KE microscope a Leica 35 mm camera was used loaded with Kodachrome X film. To improve the background illumination the camera was synchronized with a Nikon electronic flash, power unit model MS-1.

---

*This equipment was kindly loaned to us by Mr. H. Vaughan, Mettler Instrument Corporation, Princeton, New Jersey.

(U)

Figure 15. Photograph of the Mettler FP2 hot stage on a microscope within a dry bag which allows the observations to be made in an inert atmosphere.

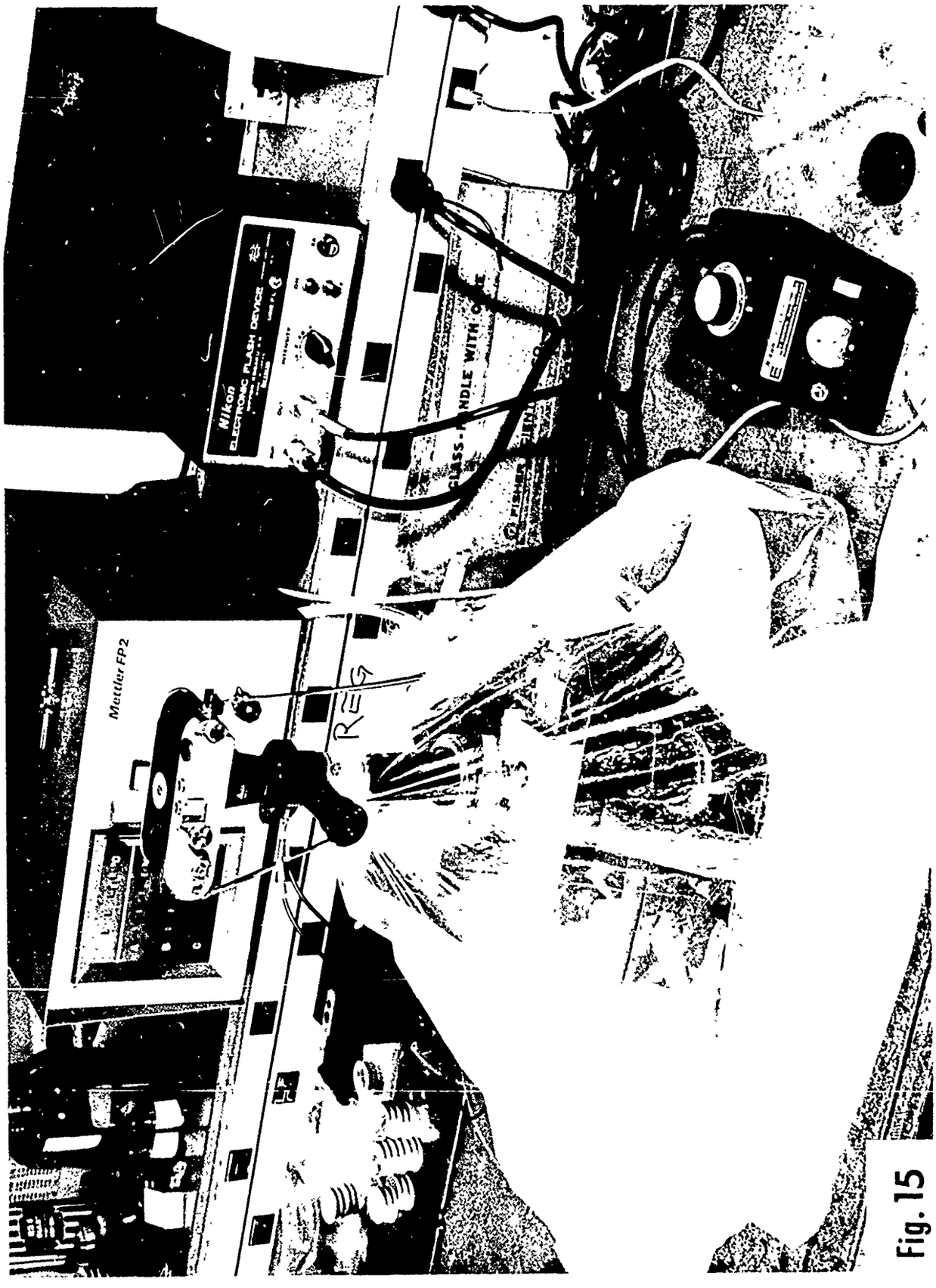

Fig. 15

2.3 Results.

2.3.1. Thermal Analysis (DTA-TGA) (U)

(U) Upon initial heating at 6°/min HAP shows two distinct low temperature endotherms occurring at about 66° and 95°C, Figure 16. The 95° peak is roughly ten times as large as the lower temperature peak and visually corresponds with sample melting.

(U) The 66° endotherm has a small but sharp weight loss associated with it. Upon cooling no corresponding exotherm is observed and neither the sharp weight loss nor the endotherm is observed if the sample is immediately reheated. Upon retesting the same sample 2 or 3 days later an endotherm is again noticed. This endotherm is lower by about 4 to 10°, has no sharp weight loss associated with it and is reproducible through at least two successive heating cycles.

(U) The sharp weight loss associated with the endothermic peak is a function of particle size. Table 7 shows weight loss values obtained with the different particle size ranges for both Navy HAP and Thiokol HAP. Navy HAP loses up to 20 times more weight than the Thiokol material with a maximum loss of 0.2% of sample weight. For Navy HAP the weight loss at the largest particle size (> 500 microns) is less than that of particles in the 354-500 micron range. This could result from formation of the largest particles by coalescence or fusing together of smaller particles but, more likely, suggests occurence of a maximum point on the weight loss curve.

(U)
Figure 16. Simultaneous DTA-TGA of Thiokol HAP (29.45 mg). The sample was held in a flowing (5 liters hour^{-1}) atmosphere of H_2C and O_2 free He and heated at 6°C min^{-1}. The phase change is recorded at 65°C and the melting of the sample at 94°C.

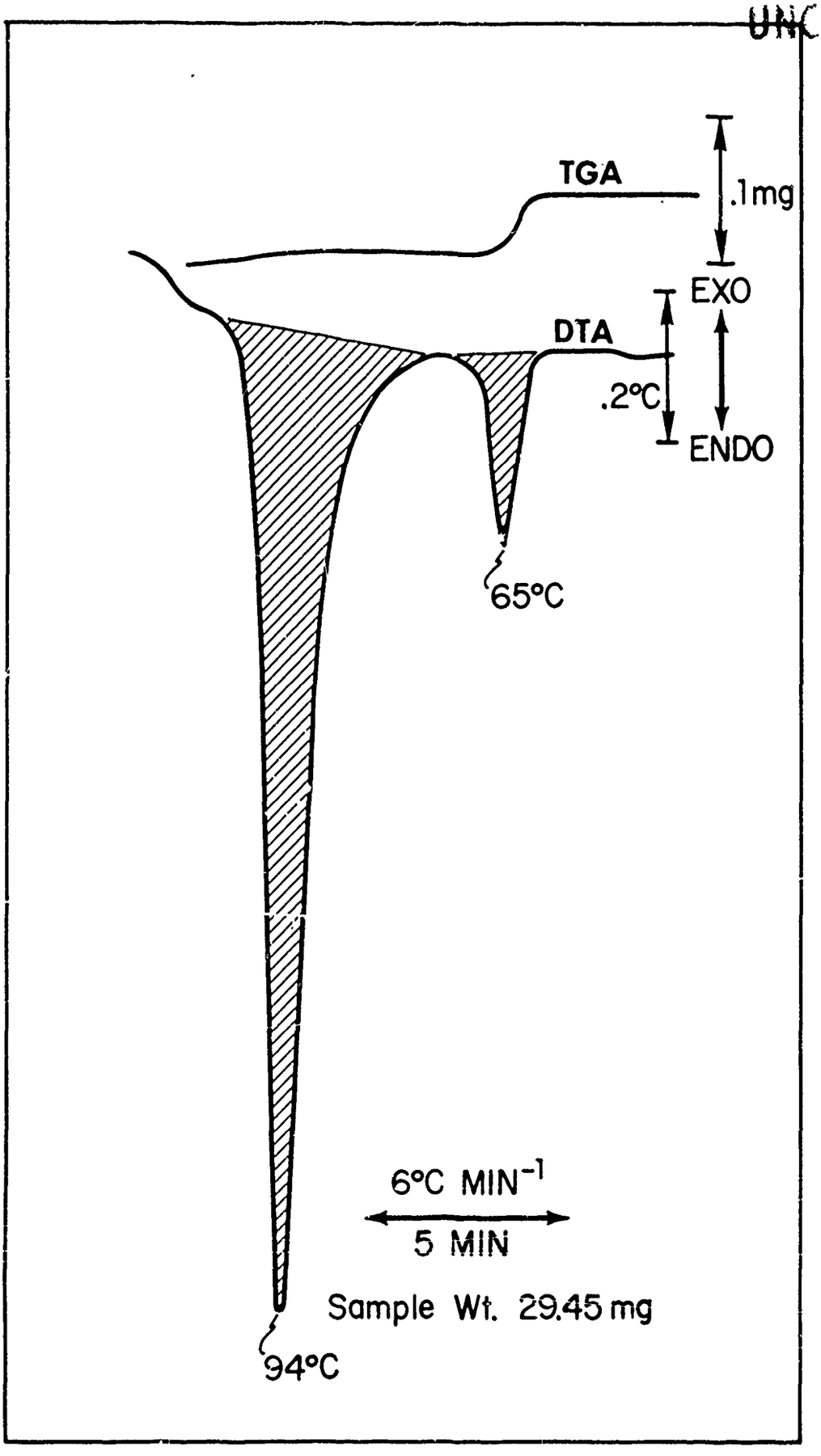

Fig. 16

(U) Other than the apparent maximum shown by the Navy HAP it is abundantly clear that larger the particle size, larger the weight loss. These data are all normalized to the same mass. If this weight loss was strictly a surface desorption then the largest effect would be seen with the smallest particle size. Our data shows that the reverse is true, which can tentatively be interpreted as an evolution from within the particles.

(U) Twenty four hours additional vacuum drying had little or no effect toward reducing the sharp weight loss of the Navy HAP and soaking the Thiokol HAP in carbon tetrachloride for 6 days did not noticeably increase its weight loss. Testing an additional sample of Navy HAP which was received in a dessicated container rather than as a carbon tetrachloride slurry gave the same type of weight loss as the main sample of Navy HAP.

(U) Enthalpy and peak temperature values for the low temperature endotherm observed with various particle size ranges of HAP are shown in Table 8. Also shown are similar data obtained for the phase transition of ammonium perchlorate from orthorhombic to cubic.

(U) With both HAP and AP a decrease in particle size results in increased DTA peak temperatures and also an increase in the estimated calories per gram values. This behavior is probably due to reduced heat conduction with the smaller particles rather than to any significant enthalpy variations. Poor heat conduction causes a higher temperature DTA peak because the center portion of the sample tends to lag behind the temperature of the sensing thermocouple. Reduced thermal conduction also results in higher thermal gradients within the sample causing the DTA peak to be broader but of

smaller amplitude. Peak height values for AP shown in Table 8 indicate this behavior. Poor conduction also increases the time required for the sample to return to ambient test temperature resulting in a larger DTA area for a given enthalpic occurance.

TABLE 7

HAP Wt. Loss for Various Particle Size Ranges* (U)

	Navy HAP			Thiokol HAP		
Particle Size (μ)	Sample Wt. (mg)	Wt. Loss (mg)	Wt. Loss ppm	Sample Wt. (mg)	Wt. Loss (mg)	Wt. Loss ppm
< 53 μ	-			539.3	0	0
53-149	31.7	1	31.5	611.1	7	11
149-210	30.0	11	367	587.1	11	19
210-354	28.5	33	1156	695.9	45	65
354-500	29.5	59	1999	468.5	45	96
> 500	34.4	53	1541	-		
	29.5	40	1356			

*These data are relevant to a $6^{\circ}C\ min^{-1}$ heating rate.

UNCLASSIFIED

TABLE 8

Enthalpy and Peak Temperature Values for Various Particle Sizes (U)

Particle Size	AP Phase Change (15 mg, 6°/min in He) Peak Temp. (°C)	Pk. Ht. (In)	Calories/g	Thiokol HAP (6°/min in Helium) Peak Temp.	Cal/g	Navy HAP (2°/min in Helium) Peak Temp.	Cal/g
< 53 μ	249	4.25	24.9	70	2.84,2.61		
53-149	248	4.41	24.0	67	3.13	63	3.72
149-210	247	4.62	22.5	67	2.49	62	3.33
210-354	247	4.55	23.7	66	2.47	62	2.97
354-500	247	4.53	23.1	66	2.67	62	3.28
> 500	246	4.55	22.9			62	2.73,2.35

UNCLASSIFIED

(U) Values of estimated enthalpy for the low temperature endotherm of HAP average about 3.06 cal/g (409 cal/mole) for Navy material and 2.71 cal/g (362 cal/mole) for the Thiokol material. The difference in values between the two batches amounts to about 12% and is of questionable significance.

(U) Vaporization energies associated with the weight loss at the phase change are so small as to be inconsequential. Weight loss with Thiokol HAP was less than the detection sensitivity during the DTA tests and the maximum loss of 60 micrograms observed with Navy HAP represents less than 0.1 cal/g (based on the heat of vaporization of carbon tetrachloride).

(U) The melting endotherm reappears upon successive heatings and during cool down of the molten material a sharp exothermic indication of freezing is indicated by a large single peak about 30% of the time and by two smaller exothermic peaks about 70%, Figure 17, of the time. In every instance the Navy Material gives a single peak in freezing. Typical temperatures and estimated enthalpies for melting and freezing of the Thiokol material are listed in Table 9. The following observations apply to Thiokol HAP.

1 - The same sample can exhibit both single and double freezing exotherms when it is cycled through the melting point.

2 - The combined area of double peaks is about the same as the area of a single peak.

3 - The initial freezing peak usually occurs between 56 and 63° irrespective of whether it is the only peak or not.

(U)

Figure 17. A DTA trace of Thiokol HAP which is heated ($6^{\circ}C\ min^{-1}$) up to its melting point at $96^{\circ}C$ and then cooled at the same rate. The two freezing points, 59° and $53^{\circ}C$ are clearly shown. The sample was in a flowing atmosphere (5 liters $hour^{-1}$) of H_2O and O_2 free He.

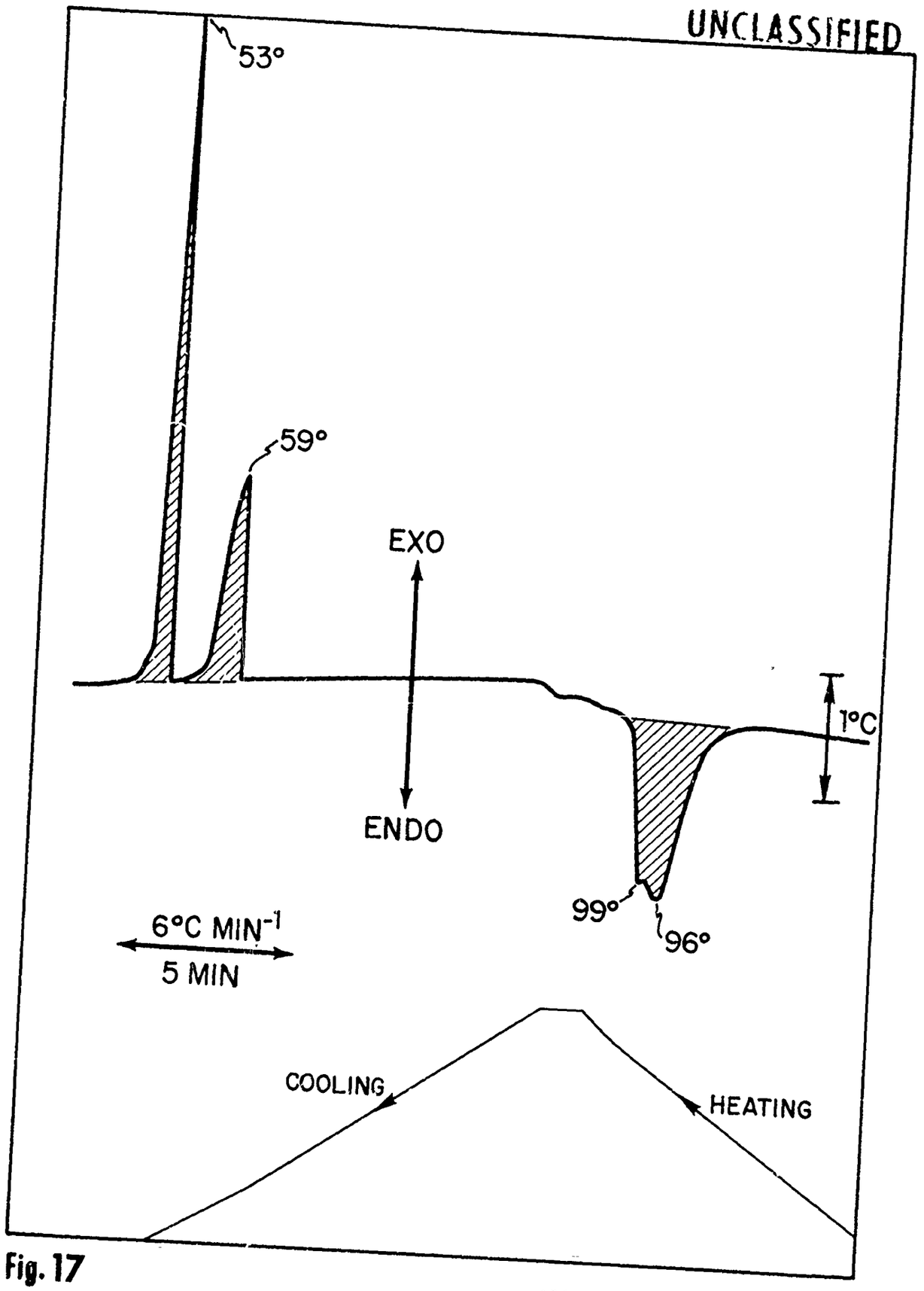

Fig. 17

TABLE 9

Temperature of Endotherm Peak and Estimated Enthalpy Melting and Freezing of Thiokol HAP (U)

Sample Wt.(mg)	Heating/ Cooling Rate °/Min	1st Heat °C	1st Heat cal/g	2nd Heat °C	2nd Heat cal/g	3rd Heat °C	3rd Heat cal/g	4th Heat °C	4th Heat cal/g	1st Cool °C	1st Cool cal/g	2nd Cool °C	2nd Cool cal/g	3rd Cool °C	3rd Cool cal/g	4th Cool °C	4th Cool cal/g
28.4	2	94	33.7	94	29.1	94	31.4			63	36.0	59	13.4	59	13.4		
												55	19.2 / 32.6	35	5.2 / 18.6		
24.3	2	94	32.5	93	30.5	92	29.1	92	29.8	64	25.8	56	40.7	59	12.9	57	14.2
														40	18.3 / 31.2	45	13.6 / 27.8
25.4	6	97	39.5	96	33.7	96	35.0			63	31.1	62	35.0	60	14.9		
														44	20.8 / 35.7		
8.6	6	95	25.3	94	23.5					56	12.5	58	8.2				
										49	16.1 / 28.6	44	15.1 / 23.3				
25.9	6/2	95	44.4	96	37.2	96	35.4	96	37.2	61	29.3	60	15.9	61	13.8	61	15.4
												59	18.5 / 34.4	52	17.3 / 31.1	60	19.7 / 35.1

UNCLASSIFIED

UNCLASSIFIED

4 - Where two peaks occur, the second (i.e. lower temperature) peak is usually larger and may occur anywhere over a fairly large temperature range (35-60°).

5 - Occurence of a double freezing does not appear related to either sample size or heating rate.

6 - The likelihood of a double peak seems to increase on successive thermal cycles.

7 - Often a small irregularity is noted in the shape of the melting endotherm suggestive of a possible double melting peak, Figure 17.

(U) The higher apparent heat content (larger DTA area) obtained upon initial melting is attributed to the poorer thermal conduction of particulate HAP as opposed to the conduction with a large fused slug of HAP.

(U) Heating of Navy material used for the low temperature endotherm study was continued up to 120° at 2°/min. Samples were then cooled and reheated at 6°/min. The melting endotherm peak was observed at the following temperatures, with a heat of fusion of 27 cal/gm.

Particle Size (Microns)	Initial Melt (2°/min)	2nd Melt (6°/min)
53-149	90°C	93°C
149-210	91	93
210-354	91	93
354-500	92	95
> 500	91	94
> 500	92	95

(U) The temperature at which the initial melting endotherm peak occurs tends to increase with particle size contrary to behavior at the lower temperature endotherm. Furthermore, this trend is repeated during the second melt where one would not expect any effect due to particle size because of previous melting and freezing. Two obvious possibilities exist:

1 - Contamination or reduced purity of the smaller particles.

2 - Some form of memory effect associated with initial freezing (e.g. more fissures or stratification occuring during freezing at the larger particles).

2.3.2. Mass Spectrometer Studies (U)

(U) Samples of Thiokol HAP have been heated up to 80°C in the direct inlet probe to a Bendix Time-of-Flight mass spectrometer. All samples were heated at 6°C/min in order to compare the data with the DTA data discussed in Section 2.3.1. In preliminary analyses it was apparent that the only unusual phenomena was a rapid increase in the H_2O^+ peak at about 65°C. This has been studied further by cyclic scanning, as a function of temperature, the m/e ranges 14-18, 14-46, 28-32, 38-46, and 0-100. Only the ranges 14-18 and 0-100 showed any unusual activity in the temperature range studied. A typical spectrum between 14 and 18 at 40°C is shown in Figure 18. From these data it is apparent that there is no unusual activity in this temperature region. Figure 19, however, recorded at 65°C, shows the rapid increase in the H_2O^+ and OH^+ peaks associated with a fairly sudden liberation of H_2O from the HAP. The agreement between the mass spectrometrically observed evolution of H_2O at 65°C and the abrupt weight losses seen by TGA at 65°C implies that these two observations are probably of the same phenomenon.

(U) Water does not reappear at 65°C if the material is thermally cycled. However, it can be observed if the material is stored for several days (~ 4 days). This undoubtedly is due to the extreme hygroscopicity of HAP thereby allowing the stored sample to pick up some water.

(U) All Navy samples tested showed an evolution of carbon tetrachloride in the region of 65°C. Naturally no water evolution was recorded since the Navy preparation is done in nonaqueous organic solvents whereas the Thiokol preparation is based on an aqueous system.

(U)

Figure 18. Mass spectrometric data for cyclic scans between m/e = 14 to 18 for Thiokol HAP held at 40°C.

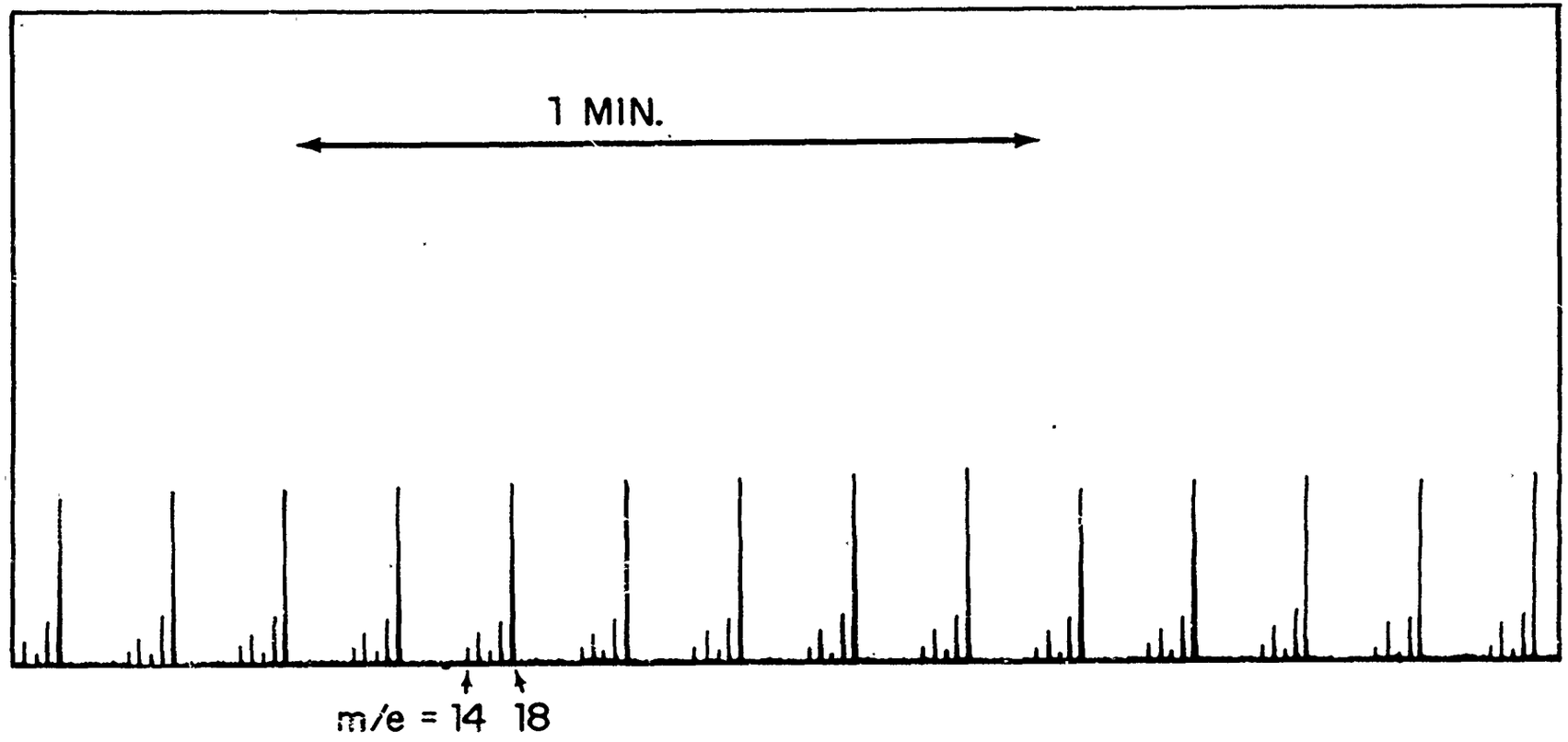

Fig. 18

(U)

Figure 19. Mass spectrometric data for cyclic scans between m/e = 14 to 18 for Thiokol HAP being heated at $6^{o}C\ min^{-1}$. The region of intense m/e = 18 peaks is at $65^{o}C$.

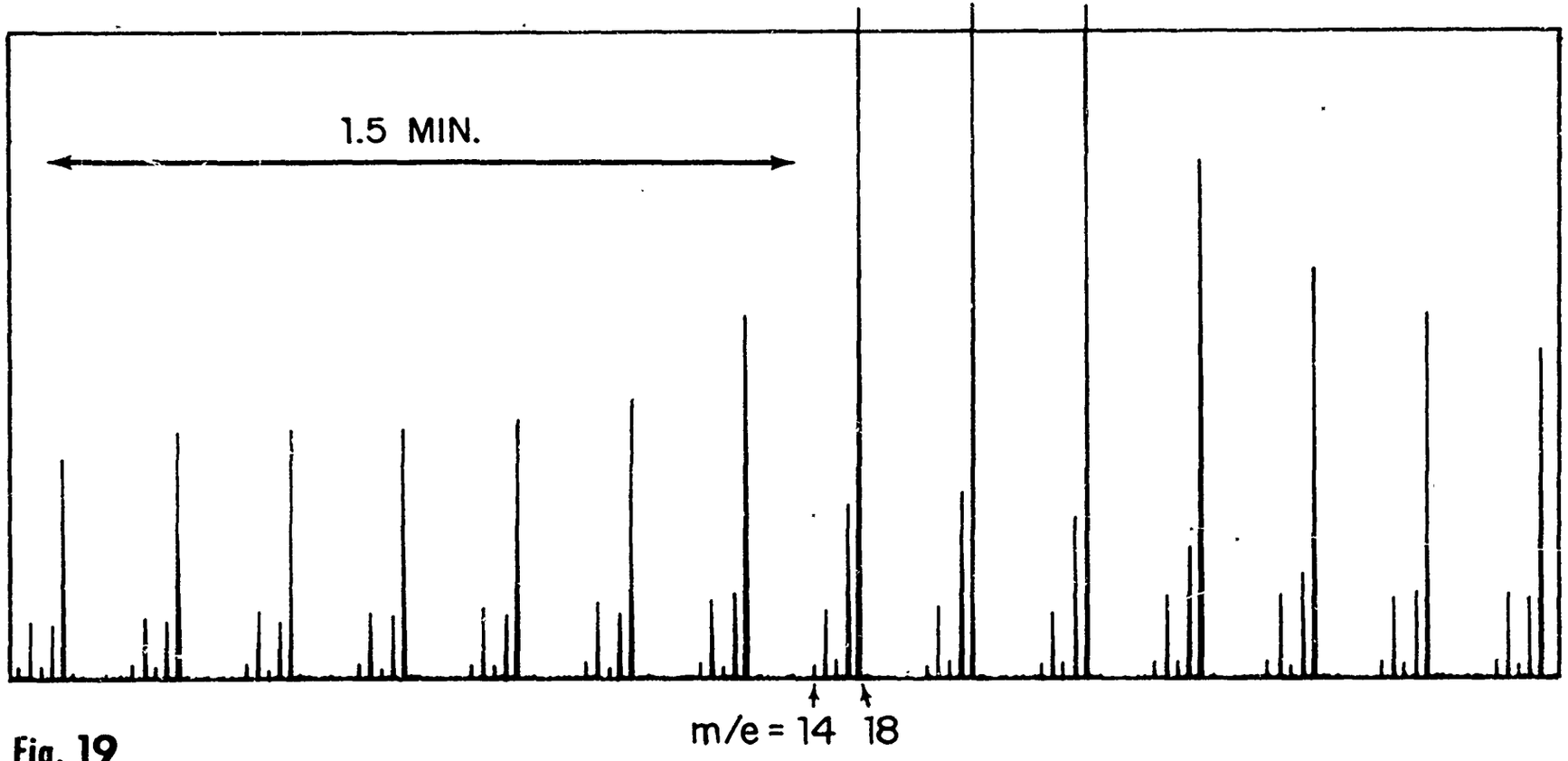

Fig. 19

2.3.3. Thermal Microscopy Studies (U)

(U) Upon heating at $2^{o}C\ min^{-1}$ samples (multicolored under polarized light) changed appearance at 55^{o}-$60^{o}C$ to give a reasonably uniformly dark image. This color transformation is best interpreted as due to a crystalline phase change. If the sample was then melted and cooled to room temperature the original multicolored state was produced. On a second heating cycle this color remained as the sample temperature passed through the range 50^{o}-$70^{o}C$ indicating that no phase change occurred. These visual observations are completely in accordance with the DTA data reported in Section 2.3.1.

(U) The melting process was invariably gradual, spread over a temperature range of $\sim 3^{o}C$, indicating the possibility of impurities present in the HAP. Freezing, at a controlled cooling rate, also appeared over a temperature range of several degrees. With the Navy HAP only one freezing point was noted. However, with the Thiokol HAP double separate freezing points were observed approximately 70% of the time. The instant at which the second solid phase forms is shown in Figure 20a. These data again are in accordance with the DTA data discussed earlier.

(U) One of the most unique features of this thermal microscopy study is that both Navy and Thiokol HAP presented an inhomogeneous appearance when molten due to the presence of a number of small dark circles which invariably appeared to have a point source of light at their center. Figures 20b and c show quite clearly the appearance just before and after melting. By comparison of these two photographs it is clear that the black circles

(U)

Figure 20. Thermal microscopy photographs, in polarized light, of Thiokol HAP. 20a is a photograph of the instant of the 2 freezing phases being clearly defined. 20b of HAP just before melting and 20c of HAP just after melting.

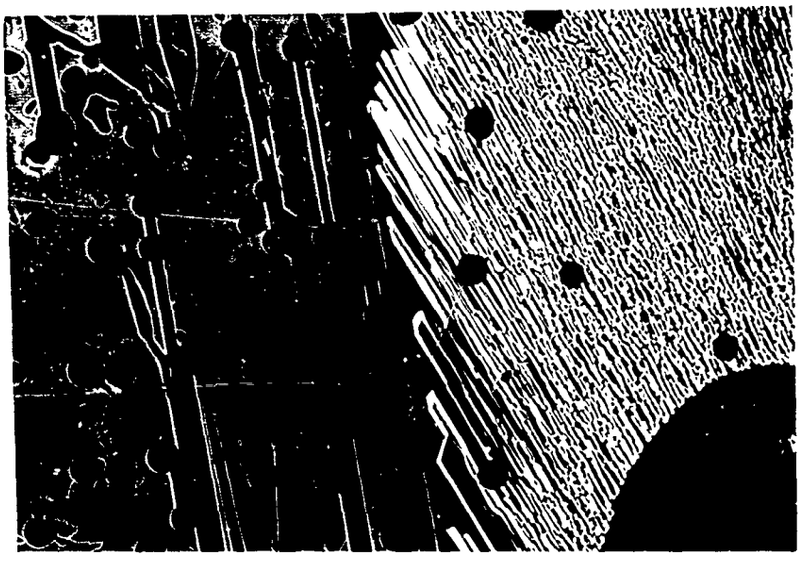

a

b

c

are not trapped gas since this can also be seen in 20°C. The circles were usually noticeable prior to melting and tended to remain visible during cool down even after freezing. The greatest number of circles was present in liquid HAP. The circles themselves were fluid and capable of uniting to form larger circles or dividing into smaller ones. On several occasions one or more of these circles were observed to spontaneously disappear.

(U) The identity of the circles is difficult to define although the fact that they show a bright center allows us to state that they are composed of a liquid having a larger refractive index than the host HAP melt. The optics for such a center is shown in Figure 21 where the idealized high refractive index bubble (a) very clearly generates an intense point source at its center when viewed along its vertical axis.

(U)
Figure 21. The physical optics of two spheres, (a) the sphere has a refractive index greater than the surrounding medium, (b) a sphere of smaller refractive index. It is abundantly clear that sphere (a) leads to the equivalent of a point source.

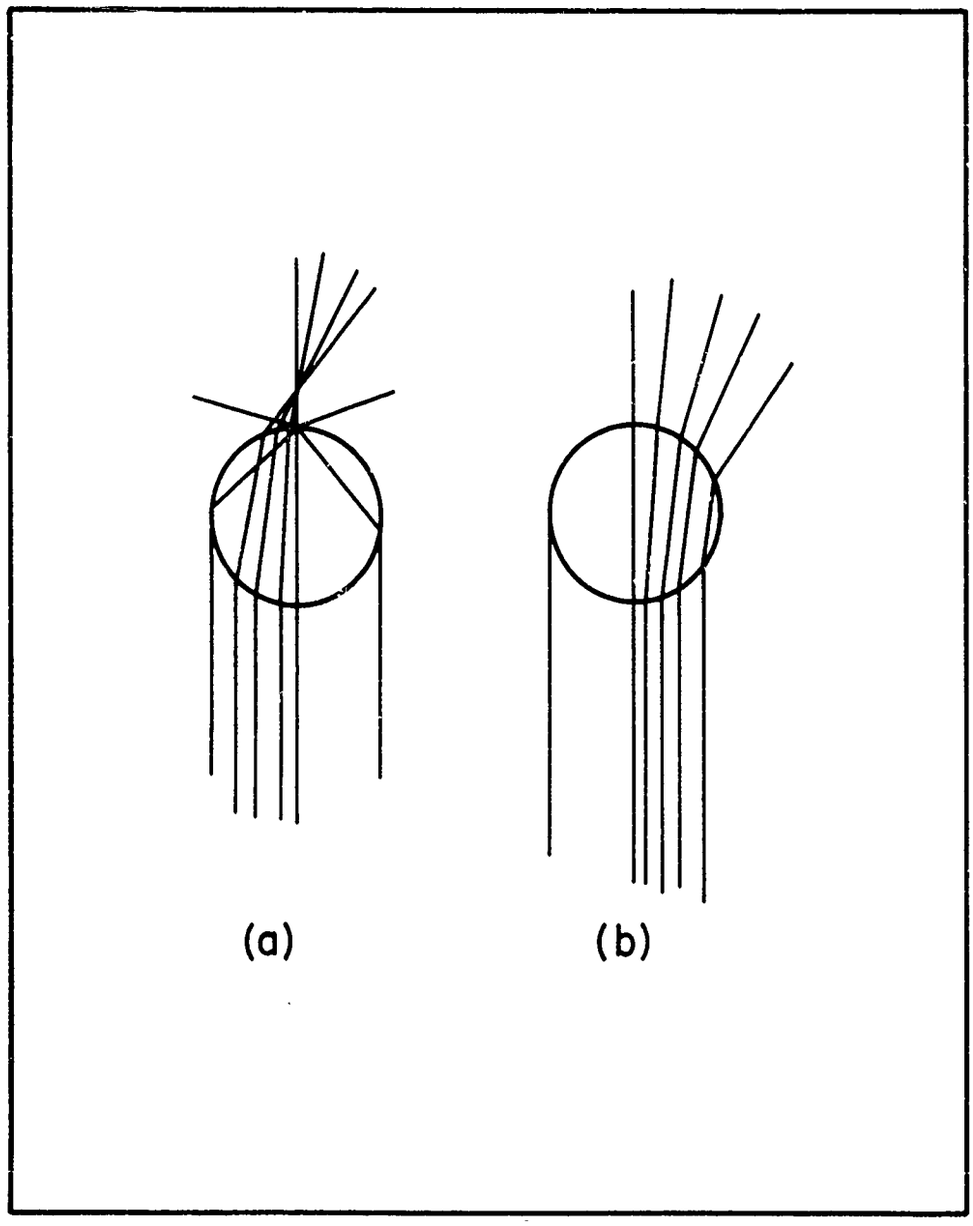

Fig. 21

2.4 Discussion. (U)

(U) The reversible low energy lower temperature endotherm is considered due to a phase transformation. The very low weight loss associated with it (0.2% maximum) makes chemical activity unlikely but is readily explainable in terms of a release of volatiles through crystal relaxation. The possibility that the endotherm results from impurity melting also exists but the absence of any associated freezing exotherm and the time delay involved in recovery are more consistent with a crystalline phase change.

(U) The origin of the carbon tetrachloride released upon an initial heating of Navy HAP is unlikely to be caused by diffusion of carbon tetrachloride into the material since the Thiokol material soaked in carbon tetrachloride did not exhibit a similar weight loss. One would, in fact, not expect the large carbon tetrachloride molecules to diffuse very readily. It must be concluded therefore that the carbon tetrachloride present in the Navy HAP occluded internally at the time of crystallization. The water which is observed in the mass spectra of both batches of material is likely due to the hydroscopic nature of HAP. Unlike carbon tetrachloride, water could be expected to diffuse readily into the HAP crystals. The appearance of water in bursts during mass spectrometer measurements suggest that water is present internally. The fact that the weight loss in parts per million for Thiokol HAP is larger with the larger particle sizes suggests that the water pick up is not a function of total surface area as much as it is a function of average volume and leads to the suspicion that some water was introduced into the Thiokol sample at the time of

crystallization. A somewhat contrary indication is given by the Navy HAP where the melting point peak temperatures suggest reduced purity for the smaller particle sizes. For a unit weight, smaller particles have larger surface areas and the evidence suggests that Navy HAP acquires some water through surface pick up. In this connection it will be noted that Baker analyzed spectrophotometer quality carbon tetrachloride contains up to 0.05% water so that the contamination might well result from prolonged exposure to carbon tetrachloride rather than to any atmospheric exposure.

(U) In the absence of evidence to the contrary both the water evolution at the assumed phase change and the more gradual weight loss sometimes observed below the melting point are attributed to a drying out of the material at elevated temperatures.

(U) The microscopic observation reinforces the conclusion that the low temperature endotherm of HAP is due to a phase change. The dark circles observed in HAP are presumed to be an effect of water although no completely satisfactory explanation is possible at present. If the dark spots are water or a water-HAP solution the question arises as to why such a phenomenon should be localized rather than uniform. The weak attractive forces between water and HAP would be affected by HAP's changing from an ionic crystal to a liquid. The assumed phase change might influence the mutual solubility of water and HAP. The circular shapes suggest that the material has a high surface tension with respect to the host HAP. The observed disappearance of these circles undoubtedly contributes to the low weight loss observed with HAP at temperatures above the phase change. The

greater incidence of dark circles in molten HAP is probably due to the greater optical clarity of molten HAP which permits one to see what previously was hidden. A less satisfactory explanation of the inhomogeneity could be based on a contaminant other than water, e.g. perchloric acid or hydroxylamine so that the observed circles represent HAP-contaminant or water-contaminant solutions. Such a contaminant could result from processing, from hydrolysis reactions or from auto decomposition.

(U) The confirmed presence of water naturally invites speculation regarding its possible effects on HAP. The drying method suggested by Thiokol of vacuum heating up to 70° suggests a weak interaction between water and HAP. A HAP sample which was allowed to dissolve itself through atmospheric moisture pick up still looked wet after 1 hour at 120° at 760 mm pressure. Should any hydrolysis reaction occur, however, it might result in the formation of perchloric acid monohydrate by a reaction such as:

$$NH_3OHClO_4 + 2H_2O \rightleftharpoons NH_4OH + H_3O\ ClO_4 + \frac{1}{2}\ O_2$$

(U) In the case of ammonium perchlorate increased reactivity has been attributed to the presence of small quantities of perchloric acid monohydrate in an earlier investigation undertaken here[16]. The reversibility of the specific reaction indicated would depend on the extent to which oxygen can diffuse out of the crystal. When oxygen is unavailable for recombination, the resulting ammonium hydroxide and perchloric acid monohydrate would combine upon melting to give AP and water.

(U) Whatever the nature of the volatiles released at the phase change it is highly probable that they will interact with the HAP-binder interface in the total propellant thus producing a change in the compatability of the system. This phenomenon will likewise give rise to a change in the activation for the thermal decomposition of pure HAP as observed by the Rocket Propulsion Laboratory.

2.5 Conclusions and Recommendations. (U)

(U) It has been clearly shown that HAP undergoes a crystalline phase change at about 60°C which is reversible after about three days. All samples of tested HAP contain occluded pockets of some high surface tension liquid, possibly a saturated aqueous solution of HAP, perchloric acid or hydroxylamine. Some volatiles are released during the phase change presumably due to the crystal relaxation. At the moment all indications are that H_2O is the major volatile released.

(U) Thiokol HAP also very clearly exhibits two freezing points which have been clearly identified as the solidification of two separate solid phases. Navy HAP does not exhibit this phenomenon.

(U) Much potential study remains to be done on HAP. The present work has indicated that water can have a measurable influence on low temperature characteristics of HAP. Further study should be directed toward measuring this water and its effect on material properties. This could be done by placing a dry sample in the thermoanalyzer and then exposing it to air. Moisture pickup would be quantitatively measured. Various combinations of heat and pressure could then be applied to the sample to evaluate effectiveness of standard drying procedures.

(U) Some verification of hypotheses developed during the current study could be undertaken. A study of the effect of additional drying and of reduced pressure on the slow steady weight loss between phase change and melting temperatures could confirm our belief that this represents a drying out of the sample.

(U) The main course of future work, however, should involve an extension of the present work to include the decomposition range of HAP. This would focus on three main areas:

(U) 1. Derivation of kinetic parameters.

2. Determination of differences attributable to batch variation, drying technique, and previous thermal history.

3. Preparation and characterization of a sample of HAP prepared by a sublimation technique.

REFERENCES

1. Zeeman, P. B. and Ritter, G. T., Canad. J. Phys., 82, 555, (1954).
2. Stecher, O. and Wiberg, E. Ber. 75, 2003, (1942).
3. Finholt, A. E., Bond Jr., A.C. and Schlesinger, H. I., J.A.C.S., 69, 1199, (1947).
4. Appel, M. and Frankel, J. P., J. Chem. Phys., 42, 3984, (1965).
5. Siegel, B., J.A.C.S., 82, 1535, (1960).
6. Breisacher, P. and Siegel, B., J.A.C.S., 86, 5053, (1964).
7. Turley, J. W. and Rinn, H. W., American Crystallographic Winter Meeting, Tucson, Arizona, February (1968).
8. Rice, J. J. and Chizinsky, G., U.S.O.N.R., Contract ONR-494(04) ASTIA No. 10696u, August, (1956).
9. Sinke, G. C., Walter, L. C., Oetting, F. L. and Stull, D. R., J. Chem. Phys., 47, 2759, (1967).
10. Maycock, J. N., Pai Verneker, V. R. and Gorzynski, C. S., Jr., J. Phys. Chem., 72, 4015, (1968).
11. "Chemistry of the Solid State", Ed. Garner, W. E., Chapter 7, Butterworth Scien. Press., London, (1955).
12. Jacobs, P. W. M. and Kureishy, A. R. T., J. Chem. Soc., 910, 4718, (1964).
13. The Dow Chemical Co. Report No. FS-4Q-66 (Final Report under Contract No. AF04(611)-11400).
14. Dickens, B., N.B.S. Washington, D.C.
15. R. Foscante, U.S.A.F. R.P.L., private communication.
16. Maycock, J. N., Pai Verneker, V. R. and Rouch, L.L., Inorg. Nucl. Chem. Letters, 4, 119, (1968).

CONFIDENTIAL
Security Classification

DOCUMENT CONTROL DATA - R & D

(Security classification of title, body of abstract and indexing annotation must be entered when the overall report is classified)

1 ORIGINATING ACTIVITY (Corporate author)	2a. REPORT SECURITY CLASSIFICATION
Research Institute for Advanced Studies Division of Martin Marietta Corporation	Confidential
	2b. GROUP IV

3 REPORT TITLE

CRYSTAL LATTICE DOPING STUDIES OF HIGH ENERGY PROPELLANT INGREDIENTS (U)

4 DESCRIPTIVE NOTES (Type of report and inclusive dates)

Final Report - May 1968 - August 1969

5 AUTHOR(S) (First name, middle initial, last name)

J. Norman Maycock
Vencatesh, R. PaiVerneker
Maclyn McCarty, Jr.

6. REPORT DATE	7a. TOTAL NO. OF PAGES	7b. NO. OF REFS
November 1969	100	16

8a. CONTRACT OR GRANT NO.	9a. ORIGINATOR'S REPORT NUMBER(S)
F04611-68-C-0068	
b. PROJECT NO. 3148	RIAS TR-69-12c
c.	9b. OTHER REPORT NO(S) (Any other numbers that may be assigned this report)
d.	

10 DISTRIBUTION STATEMENT In addition to security requirements which must be met, this document is subject to special export controls and each transmittal to foreign governments or foreign nationals may be made only with prior approval of AFRPL (RPPR/STINFO), Edwards, California 93523

11. SUPPLEMENTARY NOTES	12. SPONSORING MILITARY ACTIVITY

13 ABSTRACT (C) The kinetics of the thermal decomposition of both pure and Mg doped AlH_3 have been determined, by using both isothermal constant volume and simultaneous DTA-TGA techniques. Of most importance in these derived parameters is the fact that the activation energy for these thermal decomposition of the Mg doped AlH_3 is different from that for the pure AlH_3. To help resolve these discrepancies the electrical conductance of these same samples has also been measured as a function of temperature and time. From these two studies a model for the thermal decomposition of AlH_3 has been developed. Also reasons for the effectiveness of Mg in increasing the thermal stability of AlH_3 are presented.

(U) The thermal behavior of both Thiokol and Navy manufactured HAP has been investigated by simultaneous DTA-TGA, thermal microscopy and mass spectrometry between room temperature and 100°C. These techniques clearly establish that HAP undergoes a crystal phase change at 65° which is slowly reversible on cooling. At this same temperature H_2O is evolved, presumably due to the crystal relaxation during the phase change. A unique feature of these samples is that they contain spherical "pockets" of some material having a higher refractive index than the host molten HAP. At the moment the identity of this material is uncertain although it could be a saturated aqueous solution of HAP, perchloric acid or hydroxylamine. The poor compatibility of HAP above the crystal phase change is attributed to volatile species being liberated at the phase change. These volatiles could then disturb the HAP-binder interface bonding.

DD FORM 1 NOV 65 1473

CONFIDENTIAL
Security Classification

CONFIDENTIAL

14. KEY WORDS	LINK A		LINK B		LINK C	
	ROLE	WT	ROLE	WT	ROLE	WT
Aluminum hydride						
Hydroxylammonium perchlorate						
Differential Thermal Analysis						
Thermogravimetric analysis						
Thermal microscopy						
Electrical conductance						
Mass spectrometry						
Thermal decomposition						
Kinetics						
Decomposition models						
Doped AlH_3						
Effects of dopant						
Phase changes						
Dehydration						
Freezing points						
Activation energies						
Photochemical Decomposition						

CONFIDENTIAL

IDENTIFICATION	CURRENT STATEMENT	AUTHO
AD-387 868 [illegible] *MARTIN MARIETTA CORP BALTIMORE MD RESEARCH INST FOR ADVANCED STUDIES* [illegible] Surface of High Energy Excitation [illegible] (U) Final rept. [illegible] Aug 66, Rept no. RIAS-TR-[illegible] [illegible] Contract F04611-66-C-[illegible]	Approved for public release; distribution unlimited.	AFRPL [illegible], 10 Dec 85